

Contents lists available at ScienceDirect

Lithos

journal homepage: www.elsevier.com/locate/lithos



Research Article

⁴⁰Ar/³⁹Ar ages and bulk-rock chemistry of the lower submarine units of the central and western Aleutian Arc



Rachel Bezard ^{a,b,c,*}, Kaj Hoernle ^{c,d}, Jörg A. Pfänder ^e, Brian Jicha ^f, Reinhard Werner ^c, Folkmar Hauff ^c, Maxim Portnyagin ^{c,g}, Blanka Sperner ^e, Gene M. Yogodzinski ^h, Simon Turner ^b

- ^a Department of Isotope Geology, Goettingen University, Goldschmidtstrasse 1, 37077 Goettingen, Germany
- ^b Department of Earth and Environmental Sciences, Macquarie University, 12 Wally's Walk, NSW 2109, Australia
- ^c GEOMAR Helmholtz Centre for Ocean Research Kiel, Wischhofstrasse 1-3, 24148 Kiel, Germany
- ^d Institute of Geosciences, CAU Kiel University, Ludewig-Meyn-Strasse 10, 24118 Kiel, Germany
- ^e Geologisches Institut, Technische Universität Freiberg, Gustav-Zeuner-Str. 12, D-09599 Freiberg, Germany
- f Department of Geoscience, University of Wisconsin, 1215 W Dayton St., Madison, WI 53706, USA
- g Vernadsky Institute of Geochemistry and Analytical Chemistry, Kosigin St. 19, 119991 Moscow, Russia
- ^h School of Earth, Ocean and Environment, University of South Carolina, 701 Sumter Street, Columbia, SC 29208, USA

ARTICLE INFO

Article history: Received 21 September 2020 Received in revised form 30 March 2021 Accepted 31 March 2021 Available online 03 April 2021

Keywords: Ar-Ar geochronology Geochemistry Subduction zones Arc crust Aleutian Arc Pacific

ABSTRACT

In order to further constrain the timing of the Aleutian Arc initiation as well as its early evolution, an extensive 40 Ar/ 39 Ar dating and geochemical (major and selected trace elements) campaign (40 samples) of the lower units of the Aleutian ridge has been carried out on samples dredged from deep fore-arc canyons and rear-arc tectonic structures. The new dataset slightly increases the minimum inception age for the Aleutian system, with the two oldest samples dated at 46.1 ± 3.3 Ma and 47.80 ± 0.57 Ma. Both mid Eocene ages were obtained on tholeiitic mafic volcanic rocks from the western section of the arc. The new data also support the occurrence of three distinct periods of enhanced magmatic activity (magmatic pulses) during the pre-Quaternary evolution of the arc (at 38-27, 16-11 and 6-0 Ma), as previously suggested based on a more limited and dominantly subaerial dataset. Moreover, the data refine the duration of the first pulse of activity, which ended 2 Ma later than previous estimates. The first and last pulses may be associated with rotations of the subducting plates while the second pulse might result from regional tectonic changes. The significant overlap between the age distribution of the submarine and subaerial samples suggests that much of the earlier parts of the arc may have been uplifted and subaerially exposed. The expected crustal growth associated with the pulses is unlikely to have significantly impacted magmatic residence times, since no variation in the degree of differentiation of the rocks can be observed during or after the pulses. On the other hand, the type of magmas erupted may have changed during the arc evolution, Prior to the first pulse, activity appears to have been dominantly tholeiitic. On the other hand, the first pulse was characterized by coeval tholeiitic, transitional and calc-alkaline magmas, with calc-alkaline activity increasing after the first ~3 Ma. Subsequently, a dominantly calc-alkaline period occurred from 29 to 8 Ma, followed by a progressive return of coeval tholeiitic, transitional and calc-alkaline activity. These temporal changes in magma types correspond to likely variations in arc crustal thickness beneath the active front, and could therefore be a response to physical changes of the overriding plate.

© 2021 Elsevier B.V. All rights reserved.

1. Introduction

Since the 1960's the Aleutian Arc (Fig. 1) has been a key and extensively studied locality to understand subduction zone processes, the evolution, composition and structure of arc crusts and the link between arc and continental crust (e.g., Coats, 1962; Kay and Kay, 1994; Kelemen et al., 2003). Nevertheless, many aspects regarding its formation remain unknown or uncertain. In particular, the age at which the Aleutian Arc

crust started to develop, the evolution of its accumulation rate through time (in pulses vs. steady state) and the related impact on its magma compositions remain conjectural.

The oldest age measured so far in the Aleutians, which is also the accepted minimum inception age for the subduction system, is an 40 Ar/ 39 Ar age of 46.31 \pm 0.91 Ma (2 sigma-error here and in the rest of the manuscript; Fig. 2a) obtained on a metavolcanic rock from the submarine Murray canyon (at 3018 m depth; Jicha et al., 2006). Three

^{*} Corresponding author at: Department of Isotope Geology, Goettingen University, Goldschmidtstrasse 1, 37077 Goettingen, Germany. *E-mail address*: rachel.bezard@uni-goettingen.de (R. Bezard).

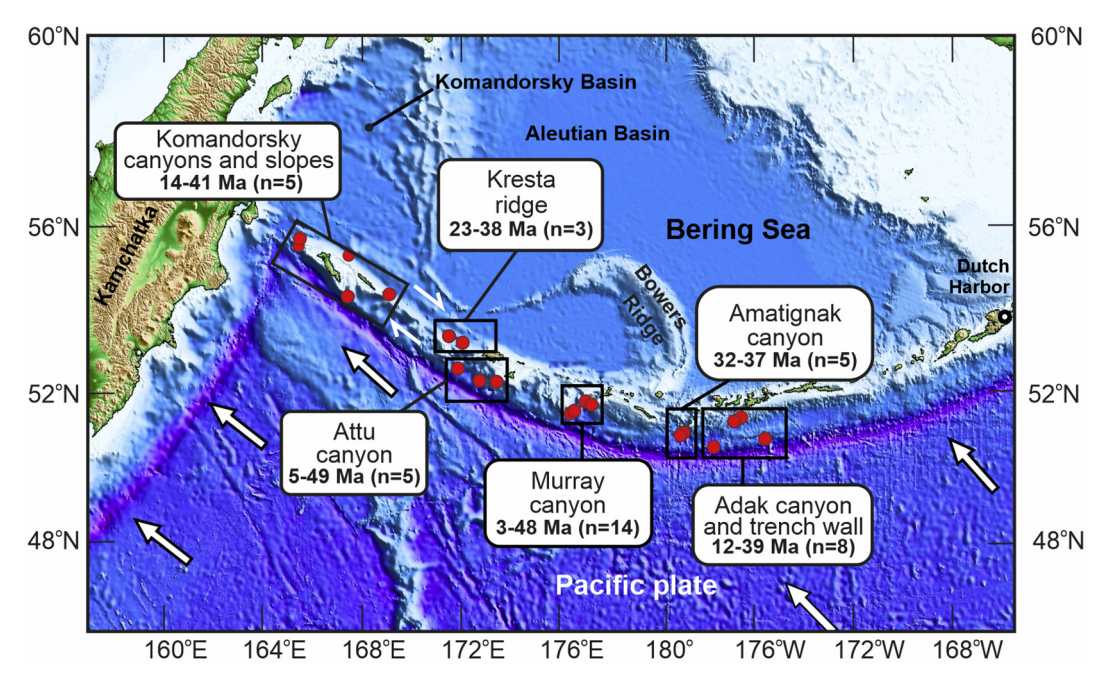


Fig. 1. Map of the western and central Aleutian Arc showing the dredge locations (red circles) from which the dated samples were recovered. The range of ages obtained for each area (taking age errors into account) is also shown. White arrows show the movement direction of the subducting Pacific plate. The bathymetric map was made using GEBCO data (GEBCO_14 Grid, v. 20,150,318; http://www.gebco.net). (For interpretation of the references to colour in this figure legend, the reader is referred to the web version of this article.)

contemporaneous or older K/Ar ages (Fig. 2) have been viewed as unreliable, in part due to their large uncertainties (55.3 \pm 6.7 Ma, 45 \pm 5 Ma and 42.3 \pm 4.6 Ma by Marvin and Cole (1978), Tsvetkov (1991) and Delong et al. (1978), respectively) and lack of reproducibility upon resampling and ⁴⁰Ar/³⁹Ar analysis. A subduction initiation age for the Aleutian arc remains unknown because rocks older than 40 Ma are scarce and come primarily from one locality. It is an important piece of the puzzle that is missing to model the Paleogene geodynamic evolution of the Pacific Basin and in particular, to understand the potential triggers for the 50-47 Ma old Hawaiian-Emperor Bend, a geological feature located south of the Aleutian arc in the central Pacific. The Hawaiian-Emperor Bend, which has been interpreted to reflect either a change in direction of the Pacific plate (e.g., Morgan, 1971; Sharp and Clague, 2006) or a change of mantle flow (e.g., Steinberger et al., 2004; Tarduno et al., 2003), is contemporaneous with the oldest Aleutian rock and has therefore been linked by some to subduction initiation in the Aleutians (O'Connor et al., 2015).

The age distribution of pre-Quaternary magmatic activity in the Aleutians also remains insufficiently constrained. Based on the available ages (Fig. 2a), the evolution of the arc has been characterized by three magmatic pulses or 'flare-ups' at 38–29, 16–11 and 6–0 Ma (Jicha et al., 2006). The number of ages, however, is not extensive (Fig. 2a) and most were obtained on samples from island outcrops, which may not be representative of the full magmatic history of the arc (see Fig. 3 for the distinction between subaerial and submarine dated samples). Moreover, despite the large amount of geochemical data generated in the last 60 years, the published geochronological data has often been obtained on samples lacking geochemical characterization, precluding a comprehensive assessment of the type of magmatism characterizing the pre-Quaternary arc evolution.

With the goals of further constraining the age of arc initiation as well as the age distribution and composition of pre-Quaternary activity, we carried out a comprehensive sampling and combined geochronological and geochemical investigation of the lower submarine units of the central and western Aleutian Arc. Sampling took place during two cruises with the German research vessel Sonne (SO249 Leg1 and 2). Combined

with the literature, the dataset provides new insights into crustal accretion and the magmatic evolution of the arc through time.

2. Geological setting

The Aleutian Arc is a ~ 2200 km long, 160-222 km wide (e.g., Holbrook et al., 1999; Lizarralde et al., 2002) arcuate ridge resulting from the subduction of the Pacific Plate beneath the North American Plate (Fig. 1). The crust has a nearly constant thickness of 38.5 ± 2.9 km in the eastern and central arc, and is likely to be as thick in the western arc (Janiszewski et al., 2013). The convergence angle changes from almost orthogonal in the eastern part of the subduction zone to oblique in the west. Due to the oblique subduction, a transtensional regime exists in the overriding plate of the centralwestern arc, resulting in the formation of northwest-southeast oriented (trench-parallel) right-lateral strike-slip faults, such as the Kresta shear zone (Scholl, 2007 and references therein). The strikeslip faults have broken the central and western Aleutian Arc basement into blocks separated by deep canyons (e.g., Adak, Amatignak, Murray and Attu; Geist et al., 1988) that have undergone clockwise rotation. The canyons provide deep basement exposures extending from the fore arc into the arc itself (Jicha et al., 2006; Scholl et al., 1982). Geophysical studies of the eastern and central part of the arc suggest that the Aleutian crust contains three layers: 1) an upper ~7 km thick layer inferred to consist of extrusive and intrusive igneous rocks of varying composition, and some volcaniclastic sediments (Holbrook et al., 1999); 2) an andesitic to basaltic mid-crustal layer made of andesitic intrusions or remnants of the oceanic crust on which the arc was built (Holbrook et al., 1999; Janiszewski et al., 2013; Shillington et al., 2004); and 3) ultramafic-mafic cumulates and/or granulites (~20-35 km; Holbrook et al., 1999; Shillington et al., 2004). This structure is broadly consistent with models based on petrological, mineralogical and geochemical data, at least for the central arc (e.g., Kay et al., 2019 and references therein). The Aleutian ridge, or arc massif, may have attained all or most of its current size (height and width) by the end of the Eocene (Scholl et al., 1987). Based on central-Aleutian

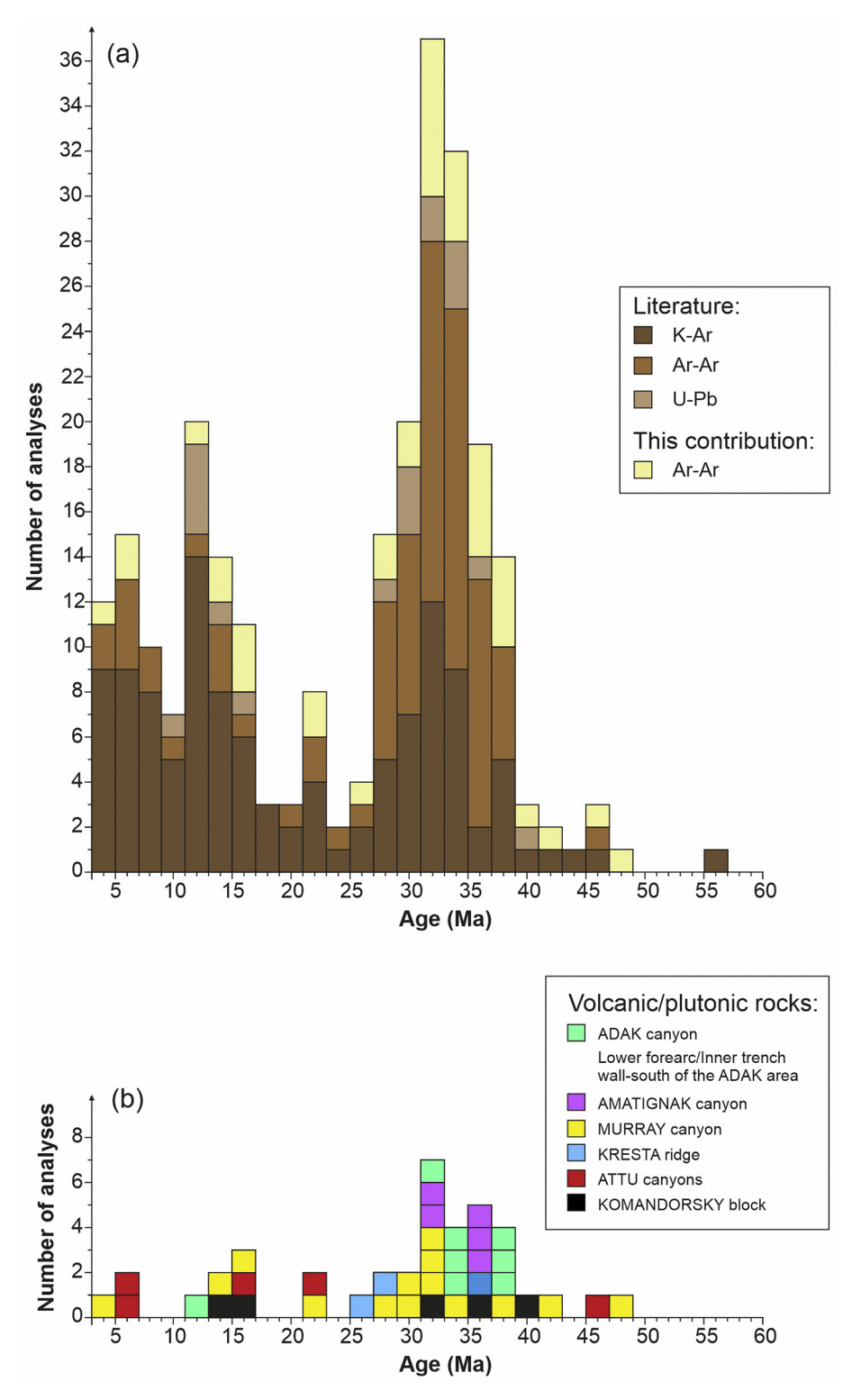


Fig. 2. Histograms showing the distribution of the ⁴⁰Ar-³⁹Ar ages obtained in this study. In (a) the new data are compared with published pre-Quaternary data for the Aleutian Islands and canyons located west of 164°W. In (b), only our new data are shown, indicating the locations from which the samples were collected. Published Aleutian data are from Borsuk and Tsvetkov (1982), Cai et al. (2015), Carr et al. (1970), Citron et al. (1980), Coombs et al. (2012), Delong et al. (1978); DeLong and McDowell (1975); Hein and McLean (1979), Jicha et al. (2006), Jicha and Kay (2018), Kay et al. (2019), Marlow et al. (1973), Marvin and Cole (1978), McLean et al. (1983); Schaen et al. (2016), Scholl et al. (1976), Tsvetkov (1991).

subaerial outcrops, early activity was likely diffuse (explaining the thick base of the ridge) and transitioned to a focused volcanic front at the end of the Eocene, e.g., at about ~34 Ma in the central arc (Jicha and Kay, 2018). The volcanic front has likely migrated

northward through time due to subduction erosion (e.g., Jicha and Kay, 2018; Kay et al., 2019; Kay and Kay, 1994). To date, the scarce number of investigated submarine outcrops has precluded a thorough understanding of the arc crustal development.

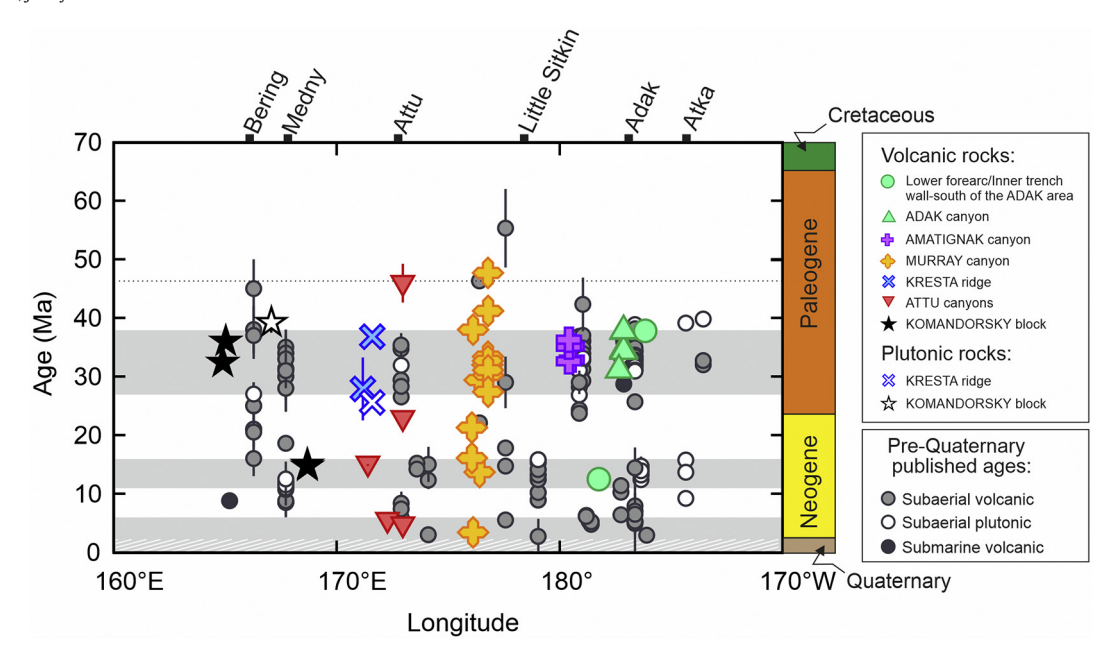


Fig. 3. Longitude of the investigated samples versus age (Ma). Other pre-Quaternary samples with published ages are shown as gray circles. The dotted line shows the previously accepted minimum inception age. The three gray fields correspond to the revised main pulses of enhanced activity of the arc. The striped gray and white field corresponds to the Quaternary part of the third pulse. Literature data as in Fig. 2.

3. Methods

3.1. Samples

Forty samples from the submarine basement of the central (east of 180°) and western Aleutians were dated and measured for major and selected trace elements. The rocks were dredged at depths between 5500 and 1000 m below sea level (mbsl) in 6 areas of the arc (Fig. 1) during the German Research Vessel Sonne Cruise SO249 in 2016. The sampling effort focused on the deep canyons cutting the fore-arc crust and extending into the arc (Adak, Amatignak, Murray, Attu and Komandorsky Canyons), on lower trench slopes (in the Adak area), and on steep slopes and faults in the rear arc (Komandorsky Block slopes and Kresta Ridge, a south-facing strike-slip fault scarp). Bathymetric maps of the dredged sites (from Werner et al., 2016) can be found in Supplementary data file 1. Several criteria were applied to minimize the likelihood of samples being ice rafted rocks (glacial dropstones). These criteria included angularity of samples, especially freshly broken surfaces, because glacial dropstones are typically rounded by glacial activity and are difficult to break by dredging. Another important criterion was the homogeneity of the rock types within a single dredge, because dropstone populations are generally very heterogeneous. After dropstone filtering, samples were selected to be representative of the dredged lithologies and, among samples of the same type, based on their freshness. More information on the content of the dredges can be found (open access) in the cruise report (Werner et al., 2016).

The sample set comprises 35 volcanic, 3 subvolcanic and 2 plutonic rocks. Individual sample descriptions are presented in Werner et al. (2016). Twenty-seven of the volcanic samples are porphyric to glomeroporphyric, and eight are aphyric. Among the porphyric/glomeroporphyric rocks, with the exception of one sample (DR49-1 from Attu Canyon), plagioclase is always present as a phenocryst. Clinopyroxene is a nearly ubiquitous phenocrystic phase, while orthopyroxene, olivine (pseudomorphs for most occurrences) and opaque oxides occur only in some of the rocks, and typically in lower modal abundances. Quartz and alkali feldspar phenocrysts are rare and only present in some of the silicic rocks (e.g., DR15-2 from

Amatignak Canyon). Amphibole phenocrysts are present in only 2 of the investigated volcanic samples (DR51-8 and DR-134-1 from Attu Canyon and Komandorsky Block slopes, respectively). In one of them (DR51-8), phenocrysts show opaque rims but are largely preserved, while in the other (DR134-1), the crystals are largely pseudomorphs. Vesicles occur in some of the volcanic rocks, and are the largest and most abundant in the aphyric samples (DR28-3, DR28-4 and DR29-24 from Murray Canyon). In most cases, they are filled with zeolites (mostly analcime) and more rarely calcite. Veins, also filled by zeolite or calcite, occur in some of the samples (e.g., DR28-4, DR51-4, DR153-9 from Murray and Attu Canyons and the Komandorsky Block slopes, respectively). Vesicle fill and veins were removed during sample preparation. Subvolcanic rocks are dominantly made of plagioclase and clinopyroxene. The assemblage of one of the plutonic rocks (DR39-8, from Kresta Ridge) is dominated by the same phases (plagioclase and clinopyroxene), but also comprises small amounts of amphibole, whereas in the other one (DR148-1, from the Komandorsky Block slopes), plagioclase and amphibole dominate the primary assemblage. The samples have undergone various degrees of low temperature subgreenschist to greenschist facies alteration.

3.2. Ar isotope measurements

Argon isotope measurements were carried out at the Argon Laboratory of the Geological Institute of the Technische Universität Bergakademie Freiberg (ALF, Germany) and at the WiscAr Laboratory in the Department of Geoscience at the University of Wisconsin-Madison (USA).

3.2.1. Argon Laboratory Freiberg (ALF)

Samples measured at ALF consisted of groundmass, feldspar and amphibole separates ranging in size from 0.12 to 0.50 mm. They were prepared by crushing, sieving and magnetic separation in some cases. The separates were handpicked under a binocular microscope and then washed in deionized water while being ultrasonicated. Some groundmass (as indicated in Table 1) and all feldspars were subsequently leached. Feldspars were leached in 5% HF at room temperature for 5 min (0.12–0.25 mm grains) or 10 min (0.25 to 0.50 mm). They were

Table 1Summary of ⁴⁰Ar-³⁹Ar incremental heating experiments.

Sample (SO249)	Location	Material	Lab	# of expts	N			³⁹ Ar %	MSWD	Plateau (Ma) ±		⁴⁰ Ar/ ³⁶ / 2σ	Ar _i ±	Isochro (Ma) ±	
DR7-3	Adak	plag	ALF	1	18	of	24	93.3	0.09	-	-	269.1	±6.1	37.90	± 0.46
DR9-4	Adak	gm	WiscAr	1	15	of	23	76.4	0.44	38.21	± 0.30	301.9	± 5.7	37.75	± 0.83
DR9-4	Adak	plag	WiscAr	1	15	of	15	100.0	0.46	38.3	± 1.4	302.1	± 3.4	37.1	± 1.9
DR9-6	Adak	gm	WiscAr	1	29	of	38	85.2	0.82	34.51	± 0.17	295.5	± 3.6	34.85	± 0.43
DR9-11	Adak	plag	WiscAr	1	13	of	17	93.8	0.61	33.0	± 1.7	290	± 11	34.6	± 2.6
DR9-16	Adak	plag	ALF	1	10	of	21	65.1	1.60	_	_	276.8	± 2.5	34.40	± 0.86
DR9-21	Adak	gm	WiscAr	1	16	of	16	100.0	0.64	38.10	± 0.25	299.9	± 3.9	37.92	± 0.58
DR10-1	Adak	gm (NL)	ALF	1	6	of	15	73.8	0.74	_	_	287.7	± 1.0	31.19	± 0.77
DR11-1	Adak	gm	WiscAr	2	22	of	23	99.9	0.98	12.83	± 0.18	302.5	± 6.3	12.58	± 0.44
DR15-2	Amatignak	plag	ALF	1	17	of	22	97.3	0.52	_	_	268.8	± 2.8	35.26	± 0.42
DR15-3	Amatignak	gm	WiscAr	1	35	of	53	72.5	0.84	32.81	± 0.09	295.7	± 3.9	32.95	± 0.23
DR16-1	Amatignak	gm	WiscAr	2	17	of	29	84.6	0.65	32.98	± 0.19	300.6	± 2.6	32.69	± 0.43
DR16-2	Amatignak	gm	WiscAr	1	15	of	42	55.1	0.66	35.09	± 0.19	297.4	± 5.0	35.21	± 0.54
DR16-4	Amatignak	gm	WiscAr	1	28	of	32	95.3	0.66	36.01	± 0.32	296.7	± 3.1	36.44	± 0.76
DR25-10	Murray	plag	ALF	1	10	of	25	53.0	1.70	_	_	292.1	± 2.3	32.11	± 0.77
DR26-1	Murray	plag	ALF	1	12	of	21	70.6	0.79	_	_	261.0	± 5.1	38.07	± 0.52
DR26-8	Murray	gm (NL)	ALF	1	16	of	18	99.4	0.29	_	_	298.2	±2.4	3.50	± 0.64
DR27-1	Murray	plag	WiscAr	1	17	of	17	100.0	0.55	27.8	± 2.1	287	± 18	29.5	± 3.2
DR27-5	Murray	gm	WiscAr	1	10	of	23	60.9	0.82	14.25	± 0.07	334	±50	13.83	± 0.59
DR28-1	Murray	gm	ALF	1	11	of	17	68.8	1.50	_	_	280.3	± 2.1	33.54	± 0.87
DR28-3	Murray	gm	WiscAr	1	14	of	14	53.8	0.70	47.70	± 0.11	295	± 18	47.80	± 0.57
DR28-4	Murray	gm	WiscAr	1	18	of	35	52.6	1.30	32.84	±0.27	299	±18	32.8	±1.3
DR29-16	Murray	plag	WiscAr	1	20	of	20	100.0	1.12	30.20	±0.37	297.7	±2.8	30.45	±0.92
DR29-21*	Murray	gm	ALF	1	11	of	22	57.7	0.10	-	_	_	-	31.16	± 0.37
DR29-22	Murray	plag	WiscAr	1	35	of	48	80.3	0.89	26.84	± 0.39	296.7	± 3.5	27.5	±1.3
DR29-24	Murray	gm	WiscAr	1	22	of	34	72.3	1.39	41.52	±0.39	299.6	± 4.1	41.3	±1.0
DR32-1	Murray	plag	ALF	1	18	of	19	99.5	1.40	_	_	296.8	±4.5	16.21	± 0.42
DR32-5	Murray	gm (NL)	ALF	1	10	of	16	61.3	0.89	_	_	261.8	±4.5	21.42	±0.98
DR32-5	Murray	plag	ALF	1	10	of	15	76.3	1.20	_	_	271.3	±3.5	19.8	±2.2
DR39-8	Kresta	plag	WiscAr	2	29	of	31	98.3	0.84	25.75	± 0.21	298.8	±1.6	25.66	±0.65
DR39-10	Kresta	gm	WiscAr	2	32	of	34	98.5	0.51	36.85	± 0.74	298.5	±1.0	36.9	±1.0
DR41-1	Kresta	plag	WiscAr	2	20	of	28	84.2	0.87	30.0	±1.4	299.4	±2.2	28.0	±5.4
DR48-1	Attu	gm	WiscAr	2	24	of	28	91.9	0.63	15.29	±0.12	298.6	±1.7	15.29	±0.14
DR49-1	Attu	gm	WiscAr	1	18	of	18	100.0	0.58	5.89	± 0.39	299.1	±1.1	5.72	± 0.54
DR51-4	Attu	gm	WiscAr	1	19	of	33	72.2	0.80	43.4	±1.1	295.5	±3.6	46.1	±3.3
DR51-8	Attu	amph	WiscAr	1	16	of	16	100.0	0.25	5.46	± 0.44	299.3	± 6.4	5.41	± 0.60
DR51-16	Attu	gm	WiscAr	1	23	of	26	93.9	0.49	21.86	± 0.47	296.7	±2.2	22.8	±1.2
DR134-1	Komand.	gm (NL)	ALF	1	13	of	20	69.5	0.99	-		294.6	±3.5	14.78	± 0.40
DR134-2	Komand.	gm (NL)	ALF	1	19	of	27	71.6	0.93	_	_	296.0	±6.8	15.11	± 0.75
DR148-1	Komand.	amph (NL)	ALF	1	9	of	19	52.4	1.00	_	_	302.1	±7.5	39.3	±1.7
DR153-9	Komand.	gm	ALF	1	8	of	22	50.3	0.80	_	_	317.4	±6.3	36.11	±0.33
DR155-1	Komand.	gm	ALF	1	12	of	23	54.7	0.66	_	_	302.8	±5.3	32.54	±0.67

Ages calculated relative to 28.201 Ma Fish Canyon sanidine standard (Kuiper et al., 2008) using 40 K decay constants of 5.463 \times 10⁻¹⁰ a⁻¹ (Min et al., 2000).

Atmospheric $^{40}\text{Ar}/^{36}\text{Ar} = 298.56 \pm 0.31$ (Lee et al., 2006); $(^{40}\text{Ar}/^{36}\text{Ar})_i = \text{initial }^{40}\text{Ar}/^{36}\text{Ar}$ ratio.

of expts = number of incremental heating experiments performed on a given sample; N = number of incremental heating steps.

Uncertainties are given at the 95% confidence level (2 σ).

 $MSWD = mean\ square\ of\ weighted\ deviates;\ gm = groundmass;\ plag = plagioclase;\ amph = amphibole;\ Komand. = Komandorsky;\ (NL) = not\ leached.$

ALF = Argon Laboratory Freiberg; WiscAr = Geochronology laboratory at the University of Wisconsin-Madison.

then rinsed and ultrasonicated in deionized water three times for 10 min at 65 °C followed by two rinses at room temperature. Ground-mass leaching consisted of three steps, all performed during ultrasonication at 65 °C: (1) 30 min in 1.8 N HCl; (2) 30 min in 0.5 N HNO $_3$; and (3) 30 min in deionized water. Between each step, the samples were rinsed 5 times with deionized water.

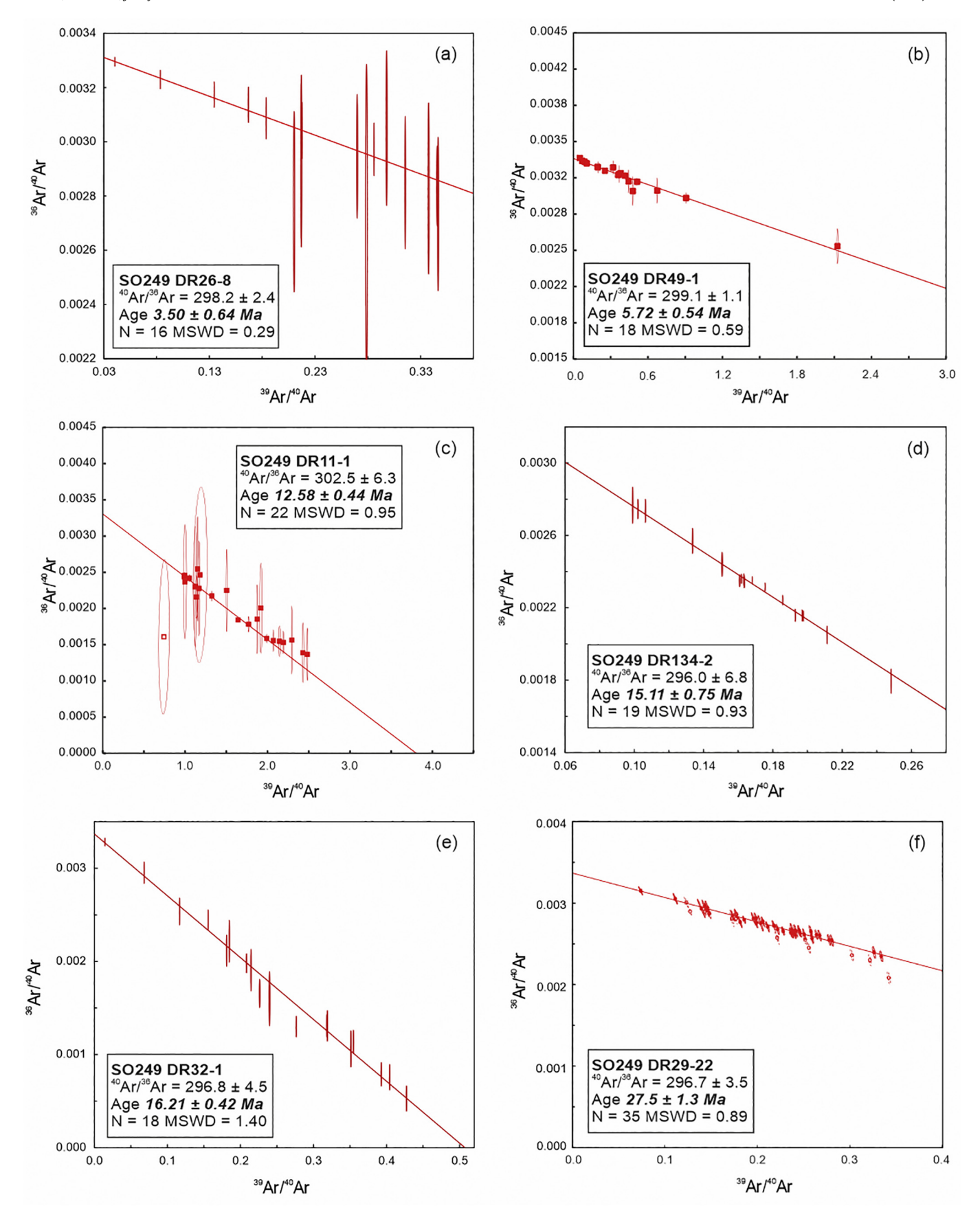
Samples were subsequently dried, wrapped in aluminum foil and loaded in wells on aluminum discs (33 mm diameter) for irradiation, which was done for 3 h at the LVR-15 research reactor of the Nuclear Research Institute in Řež, Czech Republic. The thermal neutron flux was $\sim 1.2 \times 10^{14} \, \text{n/cm}^2 \, \text{s}$ at a thermal to fast neutron ratio of ~ 2.3 . Irradiated samples were unwrapped and loaded into small Mo-crucibles for furnace step heating experiments. Step-heating was performed using a Createc high-temperature cell (HTC) controlled by an Eurotherm 3504 controller (for details see Pfänder et al., 2014). Gas purification was achieved by two GP50 getter pumps, one at room temperature and one at 400 °C. Heating and cleaning times were 10 and 7 min each per step. Argon isotope compositions were measured in static mode on a

GV Instruments ARGUS noble gas mass spectrometer equipped with five faraday cups and $10^{12}\,\Omega$ resistors for ^{36}Ar - ^{39}Ar and a $10^{11}\,\Omega$ resistor for ^{40}Ar . Typical blank levels are 2.5×10^{-16} mol ^{40}Ar and 8.1×10^{-18} mol ^{36}Ar . Measurement time was 7.5 min per temperature step acquiring 45 scans at 10 s integration time each. For raw data reduction and time-zero intercept calculation, an in-house developed Matlab® toolbox was used. Inverse isochron ages were calculated using ISOPLOT 3.7 (Ludwig, 2008). All ages were calculated using the in-house standard Drachenfels sanidine (DRFs) as a fluence monitor, with an age of 25.587 \pm 0.030 Ma relative to a Fish Canyon Tuff sanidine age of 28.201 \pm 0.046 Ma (Kuiper et al., 2008). Decay constants used are from Min et al. (2000). Reported errors on ages are 95% confidence levels (\pm 20). Interference correction factors are given in the Supplementary data file 2a.

3.2.2. University of Wisconsin-Madison (WiscAr)

Plagioclase and groundmass were isolated from the samples via crushing, sieving, and magnetic separation. Groundmass (0.18–0.25

^{*} Age derived from combination of two data subsets providing identical ages but slightly different initials. See supplementary data file 5.



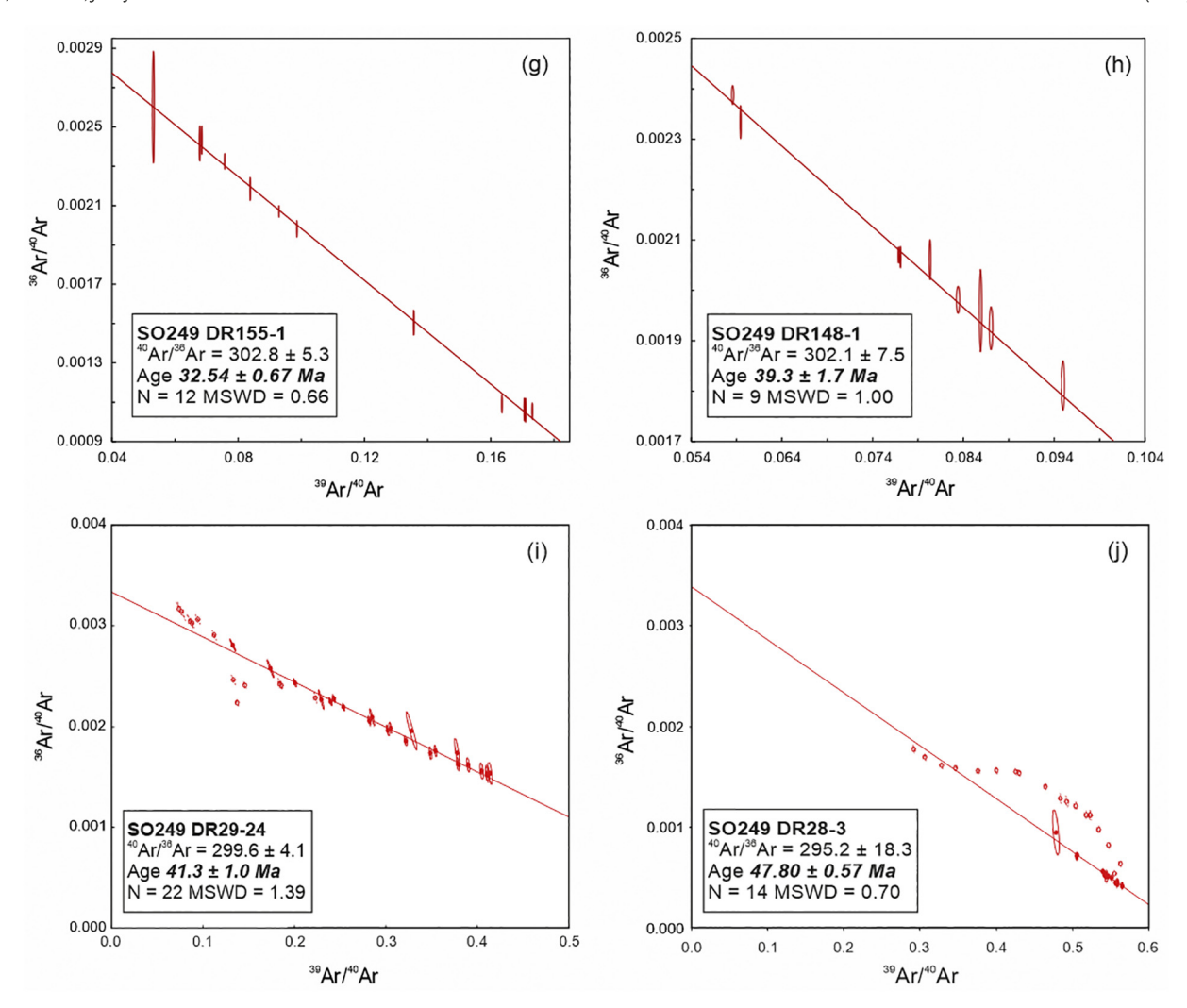


Fig. 4. Inverse isochrons for ten representative samples. Reported ages are calculated relative to a Fish Canyon sanidine age of 28.201 ± 0.046 Ma (Kuiper et al., 2008) and using a total decay constant for 40 K of 5.463×10^{-10} a $^{-1}$ (Min et al., 2000). Errors are given on a 95% confidence level (2σ). N = number of steps used for the calculation, MSWD = mean square of weighted deviates. See method section for more detail.

mm) was leached in 1.2 M HCl for 10 min, and then rinsed four times with deionized water. Following initial HCl leaching, groundmass separates were visually inspected using a binocular microscope. If alteration/secondary minerals remained, the groundmass was leached again in 3 M HCl for 10 min followed by 5 rinses in deionized water. Plagioclase separates were leached in 1.5 M HF at room temperature for 5 min (0.12–0.25 mm grains) followed by 5 rinses in deionized water. All acid leaching and subsequent rinses were done at room temperature using an ultrasonic cleaner.

Purified groundmass and plagioclase separates were wrapped in aluminum foil, placed in 2.5 cm aluminum disks, and irradiated along with the 28.201 Ma Fish Canyon sanidine standard (Kuiper et al., 2008) at the Oregon State University TRIGA reactor in the Cadmium-Lined In-Core Irradiation Tube (CLICIT). At the WiscAr laboratory, several milligrams of material were incrementally heated with a 25 W $\rm CO_2$ laser, and the released gas was cleaned during and after the heating step with two SAES C50 getters, one of which was operated at ~450 °C and the other at room temperature. Argon isotope analyses were done using a MAP 215–50 mass spectrometer following procedures outlined in Jicha and Brown (2014) or with a Nu Instruments Noblesse 5-collector spectrometer as described in Jicha et al. (2016). Blanks were analyzed after every one or two laser heating steps. The atmospheric argon value used for all calculations (40 Ar/ 36 Ar = 298.6 \pm 0.3) is from Lee et al. (2006). Reported ages are calculated using the decay constants

of Min et al. (2000) and analytical uncertainties are reported at the 95% confidence level ($\pm 2\sigma$). More information can be found is the Supplementary data file 2b,c.

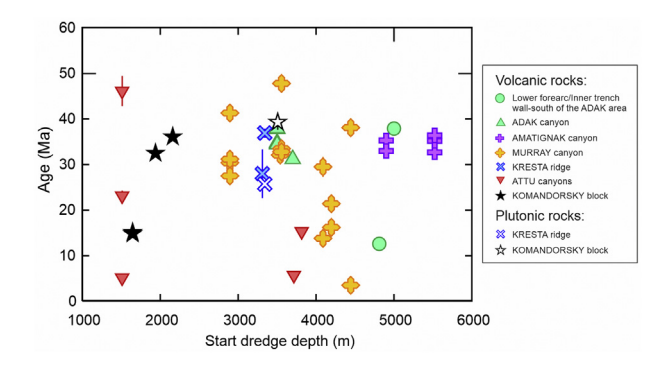
3.3. Major and trace element concentrations

Major and trace (Ba, Co, Cr, Cu, Ni, Rb, Sc, Sr, V, Y, Zn, Zr) elements were measured on fused lithium-tetraborate glass beads using the standard X-ray Fluorescence Analysis (XRF) technique at the Institute of Mineralogy and Petrography of the University of Hamburg using a PanAnalytical MagixPro X-ray fluorescence spectrometer. Loss on ignition (LOI) was determined gravimetrically at 1050 °C (Lechler and Desilets, 1987). Standards JGB-1, JB3, JB2, JA-3, JG-3 were analyzed in every batch of samples and provided concentrations typically within 3% of the values from Govindaraju (1994) for major elements and within 10% for trace elements (see Supplementary data file 3).

4. Results

4.1. 40Ar/39Ar dating

We report 42 new ages from 40 samples. The results are summarized in Table 1 and Figs. 2 and 3. Inverse isochrons for 10 representative samples are shown in Fig. 4. The detailed dataset is presented in



 $\label{eq:Fig.5.Depth} \textbf{at the start of the dredge} \, (m) \, \text{in which a sample was recovered versus sample} \\ \text{age} \, (\text{Ma}).$

Supplementary data files 2 (tables) and 4 (inverse isochrons and age spectrum diagrams).

4.1.1. Effects of alteration on the 40 Ar/ 39 Ar data

The Ar isotope compositions obtained during step-heating experiments suggest that many of the analyzed samples (groundmass, plagioclase, amphibole) are affected by post-magmatic processes such as (hydrothermal) alteration and recrystallization, which produced secondary phases accompanied by argon loss or redistribution. Despite intensive leaching during sample preparation, the presence of such phases in several samples led to no plateau on an age spectrum diagram, indicating deviation from a simple two-component mixture between closed-system radiogenic and atmospheric argon (see Supplementary data files 5 for examples). Age spectrum calculations are usually done under the assumption that the radiogenic argon component in a mineral phase is only diluted by a variable but known amount of atmospheric argon, which can be corrected, because the 40Ar/36Ar ratio in air is precisely known (298.6 \pm 0.3; Lee et al., 2006). In contrast to age spectrum plots, the calculations for inverse isochron plots do not require the knowledge of the initial argon isotope composition, but instead calculate it for all or a sub-set of the heating steps. For this study, we use inverse isochron ages as the most appropriate estimate of the age of each sample. Further explanations regarding the effect of alteration and age derivation criteria are presented in Supplementary data file 5.

4.1.2. The age data

The new ages span a large range from 3.50 \pm 0.64 Ma to 47.80 \pm 0.57 Ma. The two oldest ages, 46.1 \pm 3.3 Ma and 47.80 \pm 0.57 Ma, are contemporaneous and were obtained on samples from Attu and Murray Canyons, respectively (Fig. 2b and Fig. 3). The majority of the samples (n = 24) have ages between 27 Ma and 39 Ma. No correlation between age and dredge depth is observed, except for samples from the Komandorsky Block (Fig. 5). Both the oldest and the youngest samples came from Murray Canyon.

4.2. Geochemical results

Major and trace element concentrations obtained by XRF are presented in Table 2.

Some of the samples have undergone significant seawater alteration (e.g., three samples have LOI > 4 wt. %), which can enrich or deplete seafloor rocks in fluid-mobile elements (e.g., Pearce, 1996). No clear correlation between the major and trace elements concentrations and LOI was observed, with the one exception of LOI vs. Na_2O (not shown) forming a crude positive correlation, suggesting addition of Na by seawater. Alteration, however, generally has a variable effect on fluid-mobile element concentrations (e.g., Hart et al., 1974). Chances of heterogeneous alteration effects within the sample set are further increased due to the non-co-genetic nature of the samples, the large

geographical differences between their sampling localities and the large age differences between them. Therefore, we exclude fluid-mobile trace elements (e.g., Ba, Rb, Sr) from the discussion, and potentially fluid mobile major elements (Na, Mg, Si, K and Ca) are interpreted with care. For instance, the SiO₂ contents (Fig. 6a) of the three oldest samples (DR28-3, DR29-24 and DR51-4, from Murray and Attu Canyons) appear modified by alteration and are therefore not representative of the degree of differentiation of these rocks. Indeed, compared to the rest of the sample set, their SiO₂ concentrations are visibly enriched when plotted against Co (Fig. 6b), a fluid-immobile compatible element often used to assess the degree of differentiation of altered rocks (e.g., Hastie et al., 2007). MgO also appears affected for two of these samples (DR28-3 and DR29-24; Fig. 6c).

The dated rocks range from basaltic to rhyolitic in composition (Fig. 6). FeO, MnO, MgO and CaO tend to decrease with increasing SiO_2 , while Na_2O and K_2O tend to generally increase, although no good correlation exists (Fig. 6a, 7). Among the compatible trace elements, V, Co and Sc decrease with increasing SiO_2 , whereas Cr and Ni are highly scattered with concentrations up to 582 ppm and 179 ppm, respectively, in the more mafic samples (Table 2 and Figs. 6b, 7). Incompatible trace elements either weakly covary with SiO_2 (e.g., Zr; Fig. 7s) or do not correlate at all (e.g., Y; Fig. 7q). No overall temporal change in the degree of magmatic differentiation is obvious in the sample set (e.g., age vs. SiO_2 ; Fig. 8a).

Although the Miyashiro (1974) classification is traditionally used in Aleutian arc literature to divide subaerial samples into tholeiites and calc-alkaline rocks (e.g., Kay et al., 1990; Kay et al., 2019; Kay and Kay, 1994; Yogodzinski et al., 2015), the Ross and Bédard (2009) classification (an optimized version of the Barrett and MacLean (1999) diagram) is preferred here, because it relies on fluid-immobile elements Zr and Y instead of SiO₂ and MgO, which can be affected by seawater alteration. All mentions of calc-alkaline and tholeiitic affinities in the discussion therefore refer to the Ross and Bédard (2009) classification. Using this scheme, the dated samples range in composition from tholeiitic to calc-alkaline (Fig. 8b). The three oldest rocks are tholeiitic (Fig. 8c). Calc-alkaline rocks are found from the beginning of the first pulse (~38 Ma) until the first Ma of the third pulse (until ~5 Ma; Fig. 8c). Transitional rocks occur from the onset of the first pulse, during the first pulse and during the third pulse. Finally, with the exception of one sample, tholeiitic rocks in our sample set were produced during the early history of the arc (i.e., older than 29 Ma; Fig. 8c). We note that, excluding the three samples with visibly modified major element contents, the Miyashiro (1974) classification (Fig. 8d) is globally concurrent with this scheme (Fig. 8e). Most of the rocks classified as tholeiltic or transitional in the Ross and Bédard (2009) division are tholeiitic in the Miyashiro (1974) classification (Fig. 8e). For samples classified as calcalkaline, most discrepancies between the two schemes correspond to samples plotting on, or very close to the Miyashiro discrimination line (Fig. 8d, e), and are therefore most likely the result of classification inaccuracy and/or small alteration effects on SiO₂ for some samples.

5. Discussion

5.1. A 48 Ma minimum subduction inception age

Up to now, the oldest sample recovered in the Aleutians was 46.31 ± 0.91 Ma (Jicha et al., 2006). The oldest age obtained in our study is only slightly older outside of 2σ error (47.80 ± 0.57 Ma). As with the previous estimate, the new minimum subduction inception age clearly overlaps with the formation of the Hawaiian-Emperor Bend, formed between 50 and 47 Ma ago (Jicha et al., 2018; O'Connor et al., 2015; Sharp and Clague, 2006). While the development of Izu-Bonin-Mariana (IBM) and Tonga subduction systems at ~51–52 Ma in the western Pacific (Ishizuka et al., 2011; Meffre et al., 2012; Reagan et al., 2019) is often invoked, the development of the Aleutian Arc has also been recently viewed as a potential trigger for the formation of the

Table 2Whole rock major and selected trace element concentrations of the samples investigated (expressed in wt. % and ppm, respectively).

Sample (SO249)	DR7-3	DR9-4	DR9-6	DR9-11	DR9-16	DR9-21	DR10-1	DR11-1	DR15-2	DR15-3	DR16-1
Location	Adak	Adak	Adak	Adak	Adak	Adak	Adak	Adak	Amatig.	Amatig.	Amatig.
Lat. (°N) Long. (°W/°E) Rock type	50.786 -176.169 P volcanic	51.340 -177.134 P volcanic	51.340 -177.134 P-GP volcanic	51.340 -177.134 P volcanic	-177.134	51.340 -177.134 P volcanic	51.250 -177.350 P volcanic	50.575 -178.245 MP volcanic	-179.458	50.954 -179.458 P-GP volcanic	50.881 -179.586 P-GP volcanio
SiO ₂	67.98	50.34	55.63	52.73		49.82	51.20	52.11		65.18	50.30
Al_2O_3	14.21	18.54	16.66	18.59		18.87	20.06	16.38		15.31	16.07
FeO _T a	4.81	9.28	7.64	8.11		7.75	7.64	7.88		5.06	13.24
MgO	1.04	5.41	5.53	4.93	3.47	6.71	4.77	7.97	2.10	1.54	4.73
MnO	0.17	0.18	0.09	0.13	0.13	0.13	0.13	0.13	0.10	0.09	0.26
CaO	2.83	11.20	9.62	9.75	9.44	12.46	11.59	10.60	2.80	3.08	8.25
Na ₂ O	5.58	3.07	2.98	3.45	3.58	2.89	2.78	2.95	4.99	4.54	3.47
K ₂ O	2.23	0.71	0.97	1.02	1.34	0.55	0.44	0.77	3.33	3.68	2.07
TiO ₂	0.92	1.08	0.77	1.07	1.50	0.75	1.10	0.81	1.13	1.14	1.29
P_2O_5	0.24	0.21	0.10	0.23	0.38	0.09	0.30	0.39	0.36	0.38	0.32
LOI ^b	3.49	1.14	1.18	1.82	3.75	2.89	3.52	1.17	1.63	0.92	1.64
Mg# ^c	0.28	0.51	0.56	0.52	0.41	0.61	0.53	0.64		0.35	0.39
Ba	571	130	203	230		105	103	199		541	516
Co	7	31	30	23		39	28	34		16	35
Cr	BDL	73	94	69		350	87	336	BDL	BDL	BDL
Cu	20	181	104	149	252	131	179	88	57	64	141
Ni	BDL	30	36	35		83	37	132		1	15
Rb	67	9	8	15		8	2	10		42	31
Sc	11	28	34	23		35	29	29		12	31
Sr	187	623	464	499		439	395	454		324	427
V	52	297	248	271		271	268	240		108	461
Y	46	21	15	24	33	12	25	13	37	36	24
Zn	99	75	65	81		57	84	70		75	98
Zr	237	64	66	105	151	26	109	80	259	243	73
Sample (SO249)	DR16-2	DR16-4		DR26-1		DR27-1			DR28-3	DR28-4	DR29-16
Location	Amatig.	Amatig.	Murray	Murray	Murray	Murray		-	Murray	Murray	Murray
Lat. (°N)	50.881	50.881	51.691	51.511	51.511	51.628	51.628		51.693	51.693	51.688
Long. (°W/°E)	-179.586	-179.580		176,111		176.409			176.781	176.781	176.788
Rock type	P-GP volcar										Sub-volcanio
SiO ₂	51.87	52.74	51.32	65.45	50.20	53.41	54.42	52.86	54.18	52.27	56.03
Al ₂ O ₃	15.71	17.96	18.73	15.19	16.94	19.24	16.98	18.33	16.14	14.86	17.31
FeO _T ^a	12.54	8.46	10.07	5.54	8.22	7.53	7.06	8.31	8.97	13.55	9.74
MgO	4.55	5.75	4.07	1.56	8.22	4.26	8.11	4.77	5.81	4.55	3.47
MnO	0.30	0.42	0.17	0.07	0.13	0.11	0.13	0.13	0.26	0.31	0.20
CaO	7.87	6.14	9.17	2.90	12.26	10.90	8.31	9.53	5.08	8.58	5.22
Na ₂ O	4.23	6.17	4.56	4.33	2.48	2.53	3.24	3.20	6.53	3.51	5.25
K ₂ O	1.30	1.49	0.94	3.61	0.60	1.31	0.95	2.00	2.19	0.58	1.56
TiO ₂	1.28	0.80	0.87	0.90	0.82	0.60	0.65	0.70	0.76	1.39	1.01
P ₂ O ₅ LOI ^b	0.35	0.08	0.11	0.44	0.12	0.11	0.13	0.18	0.08	0.40	0.22
	1.44	6.65	2.34	3.29	0.83	0.31	1.49	1.43	4.78	1.40	1.73
Mg# ^c	0.39	0.55	0.42	0.33	0.64	0.50	0.67	0.51	0.54	0.37	0.39
Ba	436	60	228	698	197	186	169	263	92	350	425
Co	31	40	30	10	35	26	38	30	62	42 PDI	22
Cr	BDL	57 255	12	BDL	582	29	478	43	29	BDL	1
Cu	80	355	281	81 PDI	118	58	88 170	163	183	620	196
Ni Ph	12	43 16	8	BDL 61	149	23	179	19 17	57 22	13 7	6
Rb Sc	18	16	15 26	61	10	12	11 25	17 25	22		16
Sc Sr	29	39 224	36 408	14 275	36	29	25 277	25 610	41 67	32	28
Sr	402	234	408	275	330	816	377	619	67	492	326
V	432	241	382	82	256	225	169	244	221	457	273
Y 75	26	22	17 67	39 77	19	14	18	19 77	23	25	26
Zn Zr	50 79	77 45	67 47	77 290	69 59	57 71	72 94	77 102	171 47	128 87	81 69
Sample (SO249)	DR29-21	DR29-22	DR29-24	DR32-1	DR32-5	DR39-8	DR39-10	DR41-1	DR48-1	DR49-1	DR51-4
Location	Murray	Murray	Murray	Murray	Murray	Kresta	Kresta	Kresta	Attu	Attu	Attu
	51.688	51.688	51.688	51.508	51.508	53.271	53.271	53.405	52.605	52.282	52.260
Lat. (°N)		176.788	176.788	176.058	176.058	171.595		171.172	171.400		172.970
	176.788	1,0,,00		P volcanic	P-GP volcani						
Long. (°W/°E)	176.788 P volcanic	P volcanic	A volcanic				53.46	57.75			
Long. (°W/°E) Rock type	P volcanic	P volcanic 54.02	A volcanic 58.52		53.23	ยม.ย.			21 13	22.47	22.31
Long. (°W/°E) Rock type SiO ₂	P volcanic 56.26	54.02	58.52	57.54	53.23 19.50	60.62 16.14			51.13 17.42	52.47 17.86	52.31 15.08
Long. (°W/°E) Rock type SiO ₂ Al ₂ O ₃	P volcanic 56.26 15.10	54.02 18.33	58.52 17.43	57.54 17.41	19.50	16.14	15.41	17.03	17.42	17.86	15.08
Long. (°W/°E) Rock type SiO ₂ Al ₂ O ₃ FeO _T ^a	P volcanic 56.26 15.10 11.00	54.02 18.33 7.76	58.52 17.43 7.48	57.54 17.41 6.47	19.50 7.21	16.14 7.01	15.41 12.57	17.03 8.91	17.42 7.52	17.86 7.57	15.08 8.04
	P volcanic 56.26 15.10 11.00 3.64	54.02 18.33 7.76 4.58	58.52 17.43 7.48 5.09	57.54 17.41 6.47 4.59	19.50 7.21 4.71	16.14 7.01 3.14	15.41 12.57 5.49	17.03 8.91 3.32	17.42 7.52 7.47	17.86 7.57 7.01	15.08 8.04 7.98
Long. (°W/°E) Rock type SiO ₂ Al ₂ O ₃ FeO _T ^a MgO MnO	P volcanic 56.26 15.10 11.00 3.64 0.22	54.02 18.33 7.76 4.58 0.12	58.52 17.43 7.48 5.09 0.17	57.54 17.41 6.47 4.59 0.12	19.50 7.21 4.71 0.17	16.14 7.01 3.14 0.12	15.41 12.57 5.49 0.19	17.03 8.91 3.32 0.21	17.42 7.52 7.47 0.16	17.86 7.57 7.01 0.14	15.08 8.04 7.98 0.15
Long. (°W/°E) Rock type SiO ₂ Al ₂ O ₃ FeO _T ^a MgO	P volcanic 56.26 15.10 11.00 3.64	54.02 18.33 7.76 4.58	58.52 17.43 7.48 5.09	57.54 17.41 6.47 4.59	19.50 7.21 4.71	16.14 7.01 3.14	15.41 12.57 5.49	17.03 8.91 3.32	17.42 7.52 7.47	17.86 7.57 7.01	15.08 8.04 7.98

(continued on next page)

Table 2 (continued)

Sample (SO249)	DR29-21	DR29-22	DR29-24	DR32-1	DR32-5	DR39-8	DR39-10	DR41-1	DR48-1	DR49-1	DR51-4
Location	Murray	Murray	Murray	Murray	Murray	Kresta	Kresta	Kresta	Attu	Attu	Attu
TiO ₂	1.15	0.70	0.64	0.77	1.54	0.93	1.19	1.19	1.49	0.81	1.12
P_2O_5	0.21	0.15	0.03	0.16	0.22	0.18	0.17	0.30	0.35	0.23	0.10
LOI ^b	2.28	1.78	6.17	0.94	2.71	1.32	1.38	1.91	2.23	2.2	2.67
Mg# ^c	0.37	0.51	0.55	0.56	0.54	0.44	0.44	0.40	0.64	0.62	0.64
Ba	263	320	168	173	109	581	68	24	131	348	118
Со	27	26	60	21	28	15	33	13	33	26	53
Cr	BDL	46	38	81	43	14	BDL	BDL	181	277	335
Cu	60	225	119	53	79	36	157	49	96	55	169
Ni	3	17	74	27	20	10	11	1	122	98	55
Rb	16	26	38	7	5	23	3	BDL	5	20	BDL
Sc	33	30	40	21	24	18	40	27	23	26	40
Sr	294	597	124	490	641	473	259	106	1029	439	155
V	318	264	159	166	232	258	432	169	220	201	257
Y	30	16	12	15	18	24	24	29	20	19	25
Zn	55	56	288	59	75	41	118	87	65	63	66
Zr	75	82	34	105	124	130	56	96	154	128	55
Sample (SO249)	DI	R51-8	DR51-1	6	DR134-1	DR13	4-2	DR148-1	DR15	3-9	DR155-
Location	Attu		Attu		Komand.	Komand.		Komand.	Koma	and.	Komano
Lat. (°N)	52.260		52.260		54.348	54.348		55.269	55.63	19	55.519
Long. (°W/°E)	172.970		172.970		168.685	168.6	85	167.065	165.0	12	164.888
Rock type	P volcanic		A volcanic		P volcanic	P volc	anic	plutonic	A vol	canic	P volca
SiO ₂	57.03		55.59		58.99	60.48		47.43	58.87	,	48.81
Al_2O_3	18.01		14.32		18.63	18.93		16.58	17.35	i	19.23
FeO _T ^a	6.46		12.33		5.52	4.70		11.59	7.27		9.66
MgO	5.70		5.51		2.96	2.74		11.52	2.01		5.67
MnO	0.16		0.16		0.08	0.07		0.25	0.15		0.18
CaO	6.65		4.01		6.74	6.62		10.55	5.67		11.53
Na ₂ O	3.84		4.66		4.76	4.39		1.36	4.46		3.28
K ₂ O	1,31		2.36		1.10	1.16		0.14	2.57		0.57
TiO ₂	0.71		0.97		0.98	0.76		0.54 1.2			0.92
P_2O_5	0.		0.09		0.24	0.14		0.04	0.42		0.15
LOI ^b	3.07		8.03		1.73	1.36		1.94	1.81		2.58
Mg# ^c	0.61		0.44		0.49	0.51		0.64			0.51
Ba	15		285		104	126		70	0.33 294		170
Co	24		40		18	15		59	21		30
Cr	85		32		33	13		152	BDL		38
Cu	12		222		43	30		159	66		119
Ni	33		16		24	23		80	5		20
Rb	15		15		5	6		BDL	23		6
Sc	23		38		14	15		26	17		31
Sr	598		1042		559	713		289			497
V			356		137			195	431 167		327
v Y	206 15		356 20		157	115 10		12	34		16
zn	69		20 104		51	10 47		86	141		70
7.11	69 82		104 35		JI	47 83		30	121		25

Concentrations normalized to 100% volatile free. Amatig. = Amatignac, Komand. = Komandorsky block, Lat. = latitude, Long. = longitude. P = porphyric, GP = glomeroporphyric, MP = microporphyric, A = aphyric.

Hawaiian-Emperor Bend since it could have resulted in a change of the basal dragging force associated with the interface between the convecting upper mantle and the Pacific Plate (O'Connor et al., 2015). Our dataset reinforces the idea that such a scenario is possible. However, it would require the oldest Aleutian rock to be produced during or close to subduction initiation, and whether or not this is the case is difficult to constrain without drilling the arc basement or additional sampling via remotely operated vehicle (ROV). Comparing the compositions of the oldest Aleutian samples, which are tholeitic and lack boninitic characteristics (e.g., Ti/V = 21-26, while Ti/V < 10 for boninites (e.g., Taylor et al., 1994)), with those of rocks known to have been produced during or close to initiation of other subduction systems such as the IBM (e.g., Ishizuka et al., 2011; Reagan et al., 2010), Tonga (Meffre et al., 2012) or Matthew and Hunter (M&H) (Patriat et al., 2019) has

limitations. This is because the type of rock produced during inception is widely variable and is not unique to the first stages of a subduction system. For instance, boninite production was restricted to the first few million years after inception in the IBM but not in Tonga, where boninitic activity produced significantly later in the lifespan of the system has been identified (Meffre et al., 2012). Similarly, tholeiites thought to be contemporaneous with subduction inception in the IBM, called fore-arc basalts (FABs), can be discriminated from those erupted later based on their trace element concentrations, but this does not apply to all subduction systems. For instance, both FAB-like and typical low-Ti island arc tholeiites were erupted during initiation of the M&H subduction system. Furthermore, Guilmette et al. (2018) showed that the subduction system associated with the formation of the Semail ophiolite initiated 8 Ma before FAB-like crust was produced. Hence,

^a FeO_T = total iron as FeO.

^b LOI = loss on ignition.

 $^{^{}c}$ Mg# = molar Mg# = Mg/(Mg + Fe).

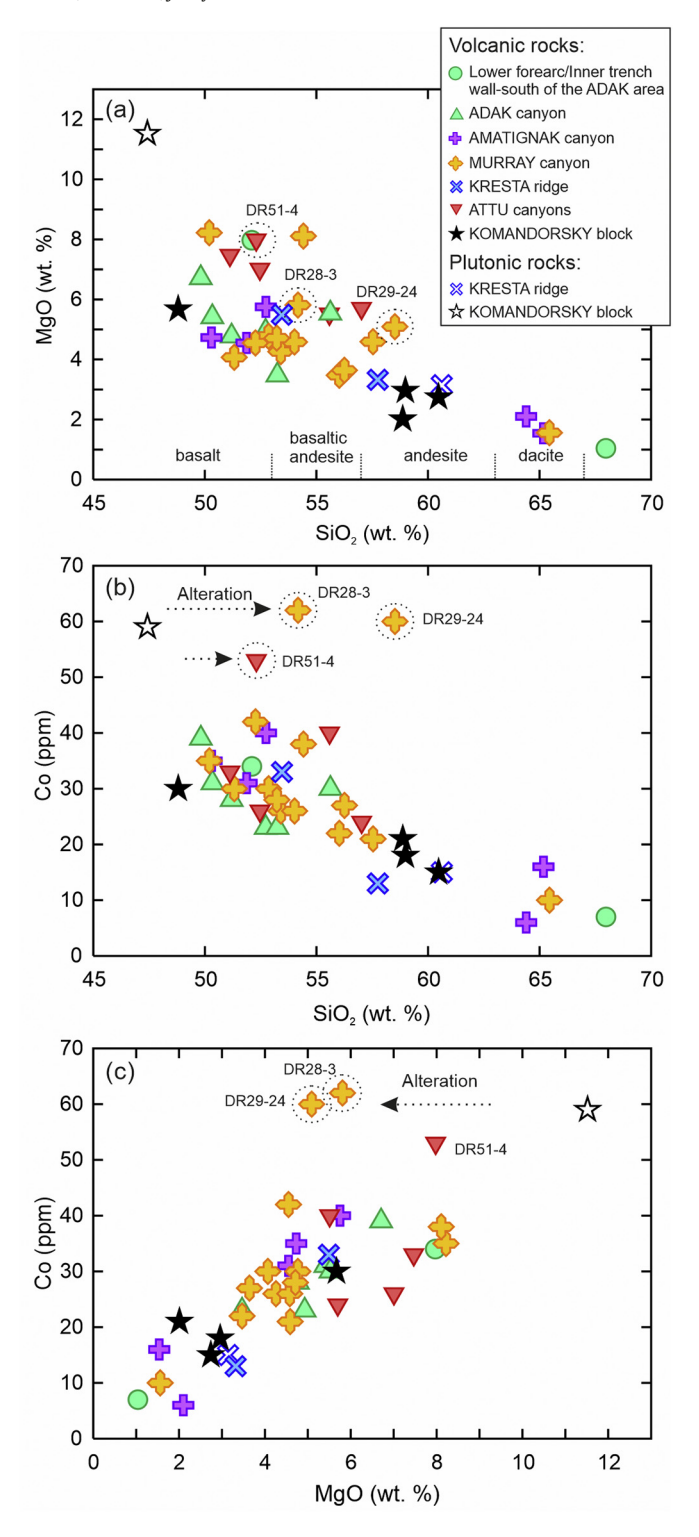


Fig. 6. (a) MgO (wt. %) versus SiO_2 (wt. %) and (b, c) Co (ppm) vs. SiO_2 (wt. %) and MgO (wt. %) for the samples investigated. The name and position (dotted circles) of three samples for which MgO and/or SiO_2 are/is inferred to be visibly affected by alteration are indicated in (a, b, c).

the compositions of the oldest Aleutian rocks alone cannot provide constraints on the timing of subduction inception.

The recovery of only two \sim 46–48 Ma samples in the fore arc (the third oldest age being 41 Ma) despite an extensive dating campaign of the submarine basement at a dredging depth of up to 5500 mbsl suggests that the oldest units are either mostly altered, not voluminous or mostly not exposed. Alternatively, the lack of voluminous older units

in the fore arc could be explained by their reworking via processes such as subduction-erosion. This process is inferred to be occurring at least in the central Aleutians, where it is associated with a northward migration of the arc and a significant reduction of the frontal units (e.g., Jicha and Kay, 2018; Kay et al., 2019). Depending on the styles of subduction initiation, crustal growth and crustal differentiation processes, the oldest crust could also have been initially volumetrically limited and/or may have been buried in the arc root by later volcanism. In any case, the scarcity of >45 Ma samples suggests that the existence of even older units is possible. Murray and Attu Canyons appear to be prime localities for further investigations since the oldest Aleutian rocks dated so far come from there (this study and Jicha et al., 2006).

5.2. Pre-Quaternary arc crust accretion and reworking

5.2.1. Three pulses of magmatic activity

Most of the ages obtained in this study fall within the three magmatic pulses previously defined for the Aleutian Arc (Jicha et al., 2006): (1) 38–29 Ma, (2) 16–11 Ma and (3) 6–0 Ma. Furthermore, the new ages occur in a similar proportion to published data (Fig. 2): the intensity of the three pulses decreases from the oldest to the youngest. This distribution (the positive correlation between pulse intensity and age in our submarine sample set) is unlikely to reflect a sampling bias associated with outcrop accessibility since older samples should be partially covered by younger rocks and be more difficult to date. Furthermore, representative samples were chosen from each dredged lithology for age determination. As can be seen in Fig. 2 and Table 1, the samples falling within the three pulses defined by Jicha et al. (2006) originate from several localities, dredges and water depths, and therefore do not reflect repeated dating of the same units. As mentioned in Section 1, the definition of the three periods of activity was made based on a dataset dominated by subaerially-exposed outcrops and, therefore, would not be expected to be representative of the age distribution of the pre-Quaternary activity. Hence, our submarine basement dataset, which significantly increases the number of pre-Quaternary data and shows the same age distribution pattern as the previous compilation, provides strong support for the occurrence of three distinct magmatic pulses during the pre-Quaternary evolution of the arc, as suggested by Jicha et al. (2006).

When coupled with the compiled literature data (Fig. 2; see caption for all literature references), the new ages suggest a protracted end to the first pulse of activity, which most likely continued until 27 Ma instead of the 29 Ma limit defined by Jicha et al. (2006). The limits of the first pulse are of particular importance because increased Pacific subduction zone volcanic activity at that time has been associated with climatic change at the Eocene-Oligocene boundary (Jicha et al., 2009). Compared to the former estimate, the updated termination age of the first pulse more closely coincides with the global increase in deep-sea temperature observed at ca. 26 Ma (suggested by oxygen isotopic records). This further supports the idea that flare-ups in circum-Pacific subduction zone volcanism may be a significant force in driving Cenozoic climate change, as suggested by Jicha et al. (2009). In addition to refining the boundaries of the first pulse, the updated dataset shows that increased igneous activity took place throughout the westerncentral Aleutian Arc during that period, i.e., from the Komandorsky block to the Adak area. Previously dated samples belonging to the first pulse were dominantly located east of 180° and west of 170°E (Fig. 3). The new data shows that increased activity also occurred between 180° and 170°E, contradicting a previous suggestion that subduction was interrupted along that section of the arc, located south and southwest of the Bowers Ridge (Fig. 1), during the first magmatic pulse (e.g., suggested interruption between 34 and 26 Ma; Vaes et al., 2019). The Bowers Ridge is an extinct arc that was active during the Oligocene (Wanke et al., 2012; Sato et al., 2016). Hence, our data shows that subduction beneath the Bowers Ridge and the adjacent part of the Aleutian Arc (170°E-180°) was occurring contemporaneously, i.e., the two

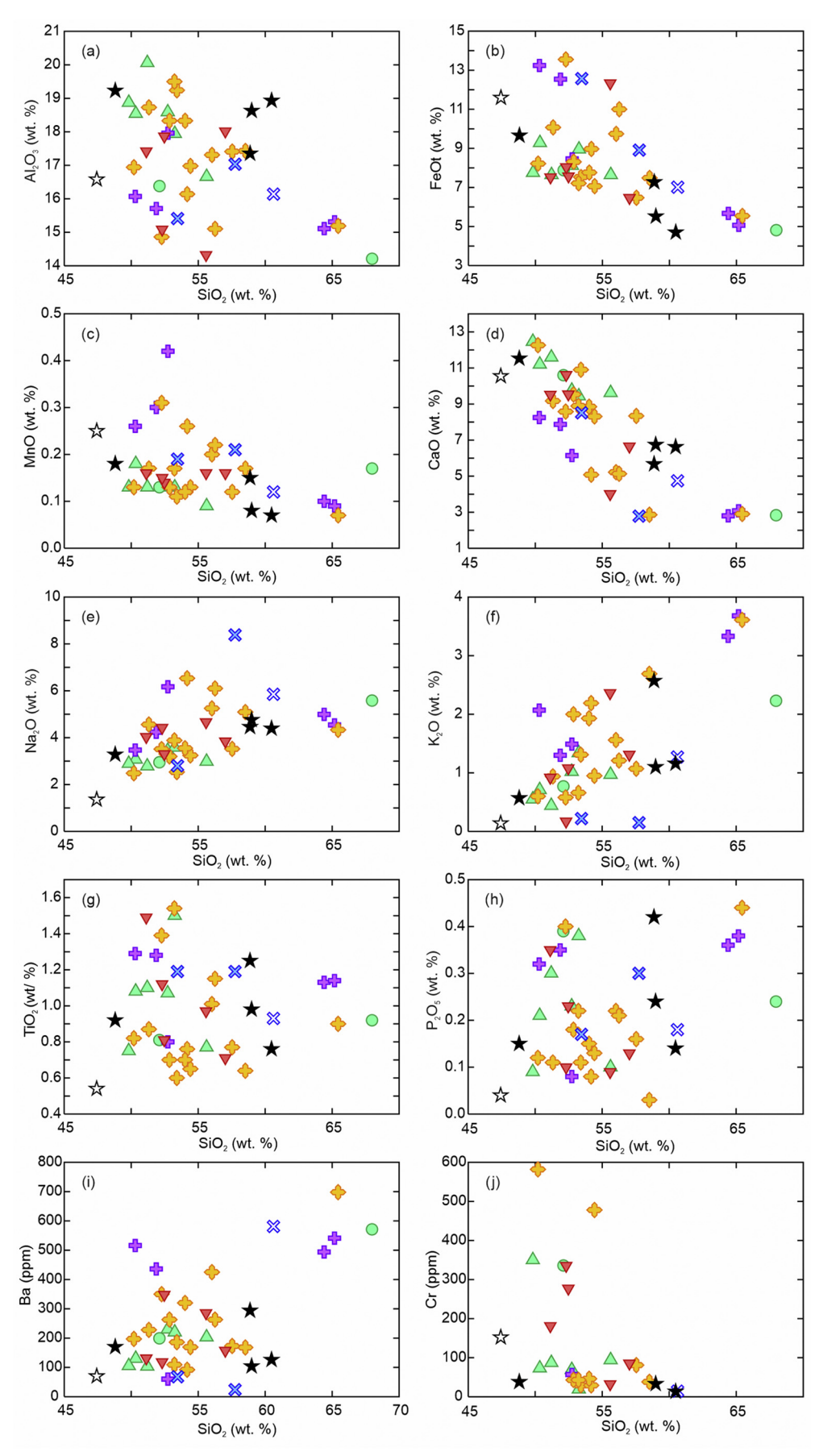


Fig. 7. Harker diagrams showing (a-h) major and (i-s) trace element variations among the dredged samples (except for MgO and Co, already shown in Fig. 6).

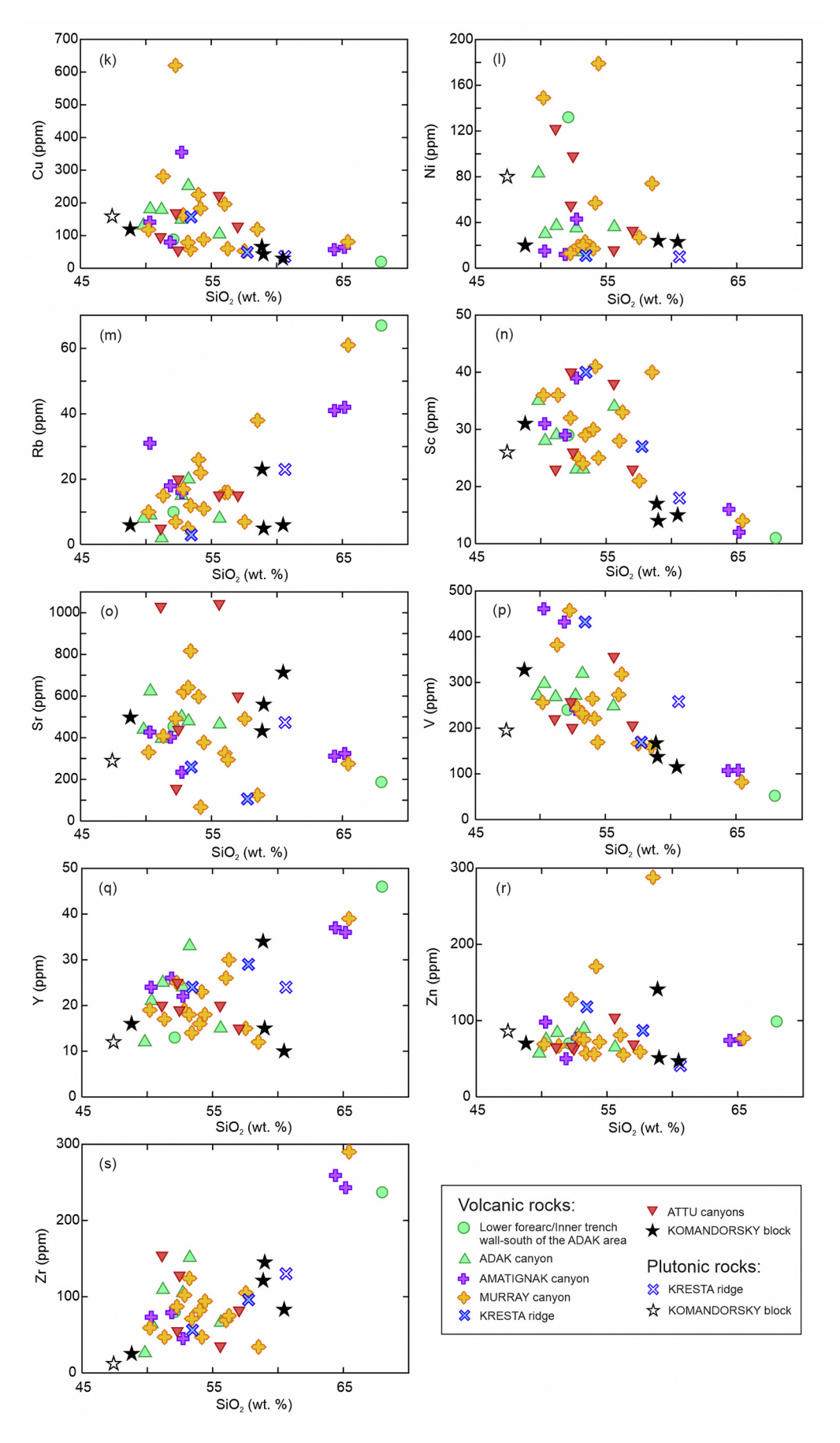


Fig. 7 (continued).

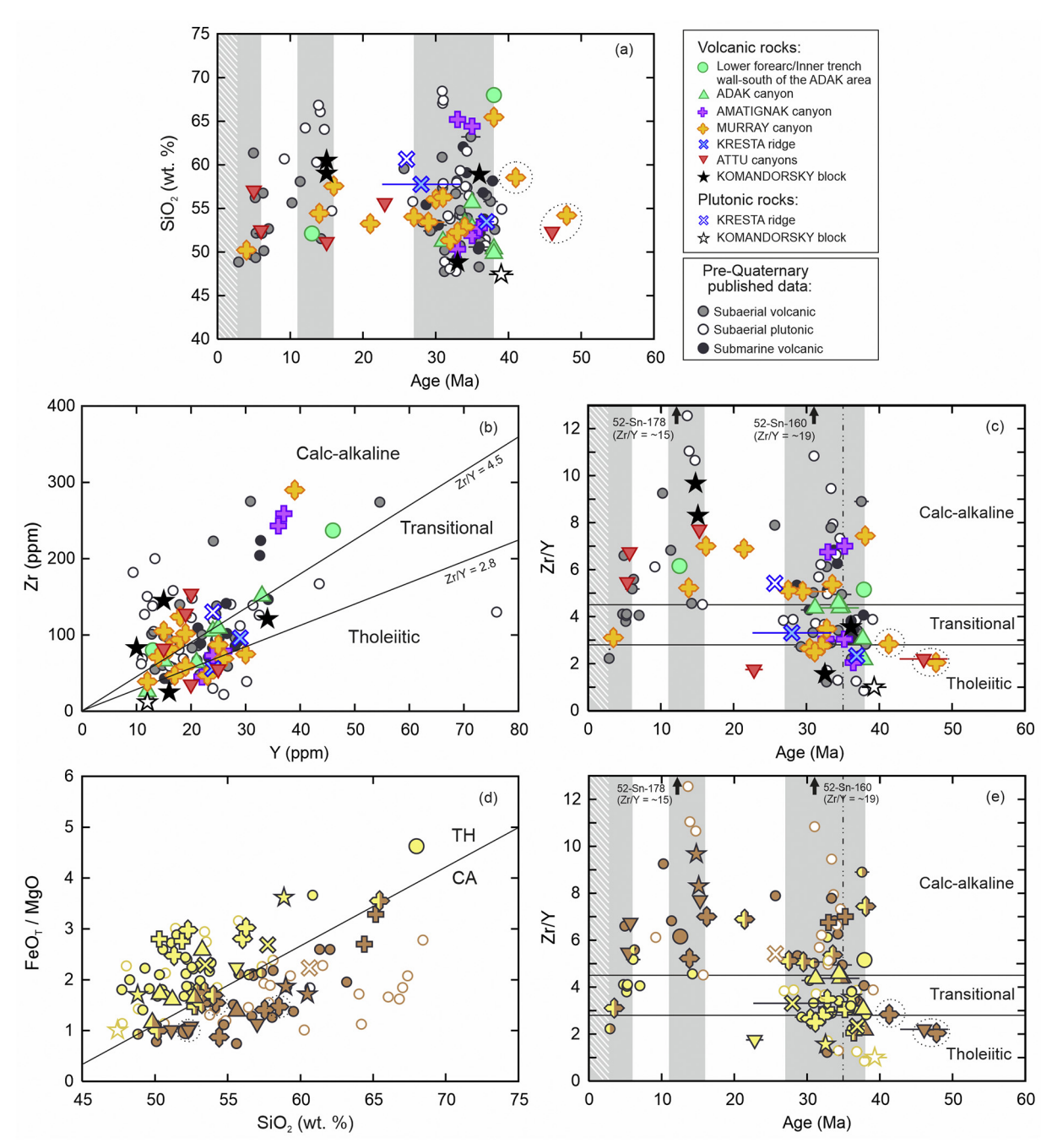


Fig. 8. (a) SiO₂ (wt. %) versus age (Ma), (b) Zr (ppm) versus Y (ppm), (c) Zr/Y versus age (Ma), (d) FeOt/MgO versus SiO₂ (wt. %) and (e) Zr/Y versus age (Ma). In (b, c, e), tholeiitic, transitional and calc-alkaline fields are separated based on Zr/Y values from Ross and Bédard (2009). In (d), the tholeiitic-calc-alkaline (TH/CA) discrimination line is from Miyashiro (1974). In (d, e) symbol shapes reflect sample locality as defined in the legend presented in (a), but the color reflects the rock type as defined by the Miyashiro (1974) classification presented in (d): yellow symbols correspond to tholeiitic rocks, brown symbols correspond to calc-alkaline rocks and symbols with both colors correspond to samples plotting on or extremely close to the discrimination line. In all panels, the three samples for which major element concentrations are visibly affected by alteration are circled (dotted circles). In (c, e), a dash-dotted line at 35 Ma, the time after which calc-alkaline magnatism began to be more important, is shown. Literature data as in Fig. 2. Out of the samples with major element data from the literature shown in (a, d), only 6 samples were not measured for Zr and Y and are therefore not shown in (b, c, e): 4 of them are calc-alkaline according to the Miyashiro definition (aged -6 Ma, 14 Ma, 31 Ma and 31 Ma) and 2 are tholeiitic (aged 31-32 Ma). Two samples from Cai et al. (2015) have Zr/Y higher than the range shown in (c, e), so their positions are indicated with arrows in these panels. (For interpretation of the references to colour in this figure legend, the reader is referred to the web version of this article.)

subduction zones co-existed during that period. As in the subaerial record, samples erupted during the second pulse were found in both the central and western arc (Fig. 3). Submarine samples belonging to the third pulse, were only found in Attu and Murray Canyons but literature data show that the activity has also been significant in the central arc (e.g., Jicha and Kay, 2018; Schaen et al., 2016). Hence the absence of activity during the third pulse only characterizes the Komandorsky Block, which is consistent with the inferred shift of the volcanic front to the

north, where it lies today and is defined by submarine edifices such as the Piip volcano (e.g., Tsvetkov, 1991; Yogodzinski et al., 2015).

Episodic rather than steady-state magmatic evolution has been recognized for all long-lived Phanerozoic continental arcs (e.g., Paterson and Ducea, 2015 and references therein) as well as oceanic arcs for which large geochronological datasets are available, such as the IBM arcs (Jicha et al., 2009). The reason for episodic, rather than steady-state, evolution of arc magmatism remains a matter of debate

and could differ among localities. Possible processes are numerous and include tectonic events causing external forcing (e.g., increase in oceanic crust production rates and/or plate reorganization; Matthews et al., 2012), regional physical changes in the overriding plate such as tectonic shortening (e.g., Ducea and Barton, 2007) or changes in the dip of the subducting plate such as slab rollback (e.g., Ferrari et al., 2007). In the Aleutians, the first pulse of activity is coeval with circum-Pacific elevated magmatic activity (at both continental and oceanic arcs) and the second and third pulses correspond to periods of intense activity in western Pacific island arcs (IBM, Tonga) (Jicha et al., 2006, 2009). Hence, at first glance, the periods of increased Aleutian activity appear linked to large-scale (e.g., Pacific-wide), rather than regional, triggers.

Based on the plate motion model of Hassan et al. (2016), a small clockwise rotation of the Pacific plate could have occurred between 35 Ma and 30 Ma, a period corresponding to the middle of the first pulse of activity in the Aleutians, followed by increasingly counterclockwise rotation between 30 and 10 Ma (see Fig. 5c of Torsvik et al., 2017). Clockwise rotation of the subducting Pacific plate would have resulted in a slightly more orthogonal convergence angle in the Aleutians, likely associated with changes in the thermal regime of the subduction zone and increases in sediment and fluid fluxes to the wedge. It could therefore explain higher magma production rates at least during the middle and the end of the first pulse (~35-27 Ma). A change in plate motion would also have the potential to affect magmatic activity at other circum-Pacific subduction zones. However, if the model is accurate, the rotation would have been small and the first pulse (~38-27 Ma) would have started before Pacific plate rotation occurred (~35 Ma). It is therefore likely that more than one factor was involved. Potential additional causes include two important tectonic changes on the subducting plate, close to the arc, just before the first pulse (~40 Ma): the end of Kula-Pacific ridge spreading (chron 18r; ~41 Ma; Wright et al., 2016) and the end of the Kronotsky arc activity (Vaes et al., 2019). These changes, or their triggers, might have had an effect on the slab, and therefore on arc magmatism.

Despite the apparent coeval increase of activity at other Pacific subduction zones (western Pacific), no large-scale tectonic change, such as clockwise rotation or speed increase of the Pacific plate, could be identified at the onset or during the second Aleutian pulse (16–11 Ma) (e.g., Hassan et al., 2016; Seton et al., 2012). On the other hand, two major regional events may have occurred in the Bering sea area just before the second pulse (~20 Ma): 1) the onset of Komandorsky basin spreading, associated with the slab pull from the proto-Komandorsky oceanic crust subducting beneath Kamchatka (e.g., Vaes et al., 2019; Yogodzinski et al., 1993); and 2) the beginning of seafloor spreading between the Bowers Ridge and the western Aleutian Ridge, associated with either Bowers (Scholl, 2007) or Aleutian (Vaes et al., 2019) slab rollback. Both spreading and slab rollback would result in renewal of hot asthenospheric mantle in the area, which could lead to increased arc magmatism in both the central and western arc. It is therefore possible that one or both of these events could have resulted in the second pulse of activity. Finally, as pointed out by Schaen et al. (2016) and Jicha and Kay (2018), a clockwise rotation of the Pacific plate motion likely occurred between 10 and 5 Ma (e.g., Hassan et al., 2016; Stotz et al., 2017) providing a suitable explanation for the third pulse of activity (6–0 Ma) observed in the Aleutian, as well as the coeval increase of activity in western Pacific oceanic subduction zones.

5.2.2. Uplift and erosion of the arc crust

The significant overlap between the age distribution of submarine and subaerial Aleutian rocks (Fig. 3) suggests that, except for activity older than 40 Ma, the submarine record of the arc may be similar to that presently exposed in the pre-Quaternary units of the islands. No evidence for slumping or landsliding can be seen on bathymetric maps of the dredged localities (see Supplementary data file 1). Furthermore, slumping would not explain the occurrence of some of the oldest

rocks in the shallowest dredges. For instance, the recovery of the ~46 Ma sample at ≤1500 m below sea level (dredge 51; Fig. 5) is nearly impossible to explain without uplift of older units. Therefore, the contemporaneous ages of rocks collected in subaerial and submarine outcrops is best explained by vertical movement of older complexes and erosion, at least at some localities. Vertical displacement of older complexes is not unexpected because, as mentioned in Section 2, the central and western Aleutian Arc crust has been reworked, at least since the Miocene, and is now dissected in blocks due to clockwise rotation accompanied by arc-parallel transtension (Geist et al., 1988).

5.3. Magma composition during arc evolution

The age distribution of the basement rocks (Fig. 2) suggests that most of the Aleutian ridge was built during its early evolution, as proposed by Scholl et al. (1987). The significant increase in crustal thickness during the first pulse of activity would be expected to affect the plumbing system of the arc. In particular, magma residence times could have increased, enhancing the production of intermediate to silicic magma compositions via crystallization and crustal assimilation (e.g., Leeman, 1983). However, as can be seen in Fig. 8a, our dataset combined with compiled literature data shows no increase in the degree of differentiation of the central and western Aleutian Arc rocks during the first pulse or between the first pulse and the subsequent activity. The same applies for the second and third pulses of activity. The range of SiO₂ covered by samples of all ages significantly overlap (Fig. 8a). Hence, if representative, the available Aleutian data set indicates that a significant increase in silicic magma production through time is unlikely to have occurred. This, in turn, suggests that the thickness of the crust is unlikely to have been a dominant control on the degree of differentiation of the pre-Quaternary central and western Aleutian Arc magmas. Similar observations and conclusions were made in other circum-Pacific systems with similar accretionary evolutions (i.e., coeval magmatic pulses; Jicha et al., 2009) such as the IBM arc (Straub, 2003).

In contrast to degree of differentiation, rock types (calc-alkaline vs. tholeiitic) may have varied through time (Fig. 8c). The compositions of the two oldest samples, from Murray and Attu Canyons, indicate that tholeiitic activity existed at the onset of the Middle Eocene in the western Aleutian Arc. The same type of activity (tholeiitic) appears to have characterized the rest of the Middle Eocene too (i.e., until the first pulse; Fig. 8c), as previously suggested by Tsvetkov (1991) based on the oldest subaerially exposed units of the arc, in the Komandorsky Islands. Thereafter, in both the central and western arc, the first pulse of activity was characterized by coeval calc-alkaline, transitional and tholeiitic magmatism (Fig. 8c), with the relative abundance of calcalkaline rocks increasing after the first 3 Ma (i.e., from ~35 Ma; Fig. 8c). This was previously observed in some of the central Aleutian Islands (e.g., Kay et al., 2019; Schaen et al., 2016) and is now shown to apply to the entire western-central arc. After the first pulse, central and western arc activity may have become almost exclusively calcalkaline until the end of the second pulse (Fig. 8c). Finally, intermediate and tholeiitic magmatic activity progressively returned, starting with coeval calc-alkaline and intermediate rocks just before and during the beginning of the third pulse (pre-Quaternary; with the exception of one tholeiitic lava; Fig. 8c) followed by coeval calc-alkaline, intermediate and tholeiitic activity during the Quaternary part of the third pulse (see Quaternary rock compositions in Fig. 4b of Yogodzinski et al., 2015). Cai et al. (2015) speculated that primitive tholeiitic and calcalkaline magmas could have been coevally produced throughout most of the pre-Quaternary evolution of the central and eastern Aleutian arc. Our study suggests that this is most likely only true for the early (until the end of the first pulse) and late (transitional rocks since ~8 Ma and tholeiitic rocks during the Quaternary) activity of the central and western arc. The lack of tholeiitic or transitional volcanic rock with an age between the end of the first pulse (27 Ma) and ~8 Ma (with the

exception of one sample) suggests that only one type of activity could have dominantly existed during this period.

Determining the cause(s) behind the temporal variations presented above is not straightforward. A large number of processes have been suggested regarding the production of calc-alkaline versus tholeiitic arc magmas (e.g., Chin et al., 2018 and references therein). For the pre-Quaternary Aleutian Arc, both source and crustal controls have been invoked. For instance, Cai et al. (2015) suggested that Cenozoic calc-alkaline plutons from the central and eastern Aleutian Arc were derived from a different type of parental melt, with higher SiO₂, fO₂ and/or H₂O than the tholeiitic rocks. This kind of model was also invoked by other authors for Miocene to recent calc-alkaline magmatism in the western Aleutians (Yogodzinski et al., 1993, 2015, 2017). On the other hand, Kay et al. (1990, 2019) and Kay and Kay (1994) suggested that tholeiitic and calc-alkaline pre-Quaternary Aleutian rocks, with the exception of rare rocks with strong adakitic signatures (high La/Yb, Sr/Y and Sr contents; Kay, 1978), are derived from similar parental magmas, with the calc-alkaline flavor developing during magmatic differentiation. In their model for the Adak region of the arc, Kay et al. (2019) suggested, based on the chemistry of plutonic rocks, that differentiation in the lower arc crust produced water-rich high-Al basalts. These basalts then either stalled in the middle-crust during ascent, where they acquired a calc-alkaline flavour via fractionation of a pargasitic amphibole-bearing assemblage, or ascended without mid-crustal stalling and amphibole fractionation, and were erupted as tholeiitic magmas. The authors suggested that calc-alkaline magmatism appeared in the central Aleutian Arc at about 35 Ma (Adak and Kagalaska) due to an increase in crustal thickness as well as the compressional stress associated with the northward migration of the magmatic front. The role of compressional stress in determining the type of magmatism in the arc has also been invoked in other studies such as Yogodzinski et al. (1993), Kay et al. (1982) or Singer and Myers (1990).

While testing the validity of the models discussed above is beyond the scope of this contribution, the increased temporal and geographical resolution of pre-Quaternary rock type distribution provided by our sample set allows the discussion of potential large-scale drivers of magma composition. One important parameter, expected to have fluctuated during the subduction zone evolution and having the potential to affect magmatism in the entire central-western arc segment, is crustal thickness. Crustal thickness has previously been inferred to control the nature of arc magmatism through crustal and/or mantle processes. For instance, as described in the previous section, Kay et al. (2019) suggested that, under compressional stress, calc-alkaline magmas formation is favoured as crustal thickness increases due to enhanced stalling of water-rich mafic melts in the middle crust. On the other hand, Chin et al. (2018), noting that calc-alkaline and tholeiitic magmas are both produced in thin juvenile island arcs while calcalkaline rocks are dominant in thicker arcs (see also Farner and Lee, 2017; Tang et al., 2018), invoked a response in the mantle wedge. More precisely, the authors suggested that the thickness of the crustal/lithospheric column controls the degree of melting in the mantle wedge, as originally proposed by Plank and Langmuir (1988). Melting degree, in turn, controls the water and Fe³⁺ contents of primitive arc melts and therefore the differentiation trend of these melts (e.g., Chin et al., 2018). The crust of the Aleutian Arc ridge is expected to have significantly thickened during the first and most important pulse of arc magmatism. Therefore, the increase in calc-alkaline activity a few (~3) Ma after the beginning of that first pulse would be consistent with a control by crustal thickness. As the crust is expected to have further thickened during the remainder of the first magmatic pulse, a control of crustal thickness on the nature of the subsequent activity would also be consistent with the change from coeval eruption of tholeiitic, intermediate and calc-alkaline rocks to calc-alkaline rocks alone at the end of the first pulse. Although other parameters with the potential to influence magma type also changed during the late Miocene, such as the decrease in compressional stress in the central and western arc

crust (e.g., Scholl, 2007), the return of transitional and tholeiitic magmas during the recent activity of the central and western arc (from about 8 Ma) could also correspond to a change in crustal thickness at the volcanic front. Indeed, volcanic activity is thought to have significantly shifted northward over the last 5 Ma (Jicha and Kay, 2018) and the locus of mantle partial melting could therefore have been shifted beneath a thinner part of the arc root.

Hence, even if other factors also operated, changes of crustal thickness throughout the arc evolution could be a potential driver for the observed changes in whole-rock chemistry (rock types) through time.

6. Conclusions

An extensive ${}^{40}\mathrm{Ar}/{}^{39}\mathrm{Ar}$ dating campaign of the submarine central and western Aleutian basement provides a revised minimum initiation age for the Aleutian Arc of 47.80 \pm 0.57 Ma, which is similar but slightly older than the previous estimate. The study significantly increases the number of pre-Quaternary 40Ar/39Ar ages from the Aleutians and supports the occurrence of three pulses of activity (at 38-27, 16-11 and 6-0 Ma), as previously suggested based on a more limited and dominantly subaerial literature compilation. The first and the last pulses possibly result from changes in direction of motion of the subducting plate, while the second pulse might be the consequence of regional tectonic processes. The coeval ages of subaerial activity and deep submarine units, as well as the lack of correlation between dredge depth and sample age are likely the consequences of tectonic reworking of the basement and erosion. The new dataset combined with the literature data suggests that Aleutian Arc magmas did not become more silicic after important periods of crustal accretion, precluding a strong control of crustal thickness on their degree of differentiation. On the other hand, some temporal variations of rock type (tholeiitic, transitional and calcalkaline) are observed and potentially result from arc crustal thickness variations.

Declaration of Competing Interest

The authors declare that they have no known competing financial interests or personal relationships that could have appeared to influence the work reported in this paper.

Acknowledgements

We thank K. Junge for her help during mineral separation and S. Jung for providing XRF data. We are grateful to the master, crew and scientific party of R/V Sonne Cruise SO249 for their excellent support on board. Jan Milcak and the irradiation services team of the Research Centre Řež, Czech Republic, are acknowledged for performing neutron irradiation of the samples dated in Freiberg. We are grateful to Mark Reagan and Suzanne Kay for their very constructive comments and Michael Roden for the editorial handling of the paper. This work was supported by BMBF (German Ministry for Education and Research) Grant for the SO249 Bering project (03G0249A) and NSF grants 1551657, 1753492, 1551640 and 1753518. RB further acknowledges support from DFG grant BE6670/1-1.

Appendix A. Supplementary data

Supplementary data to this article can be found online at https://doi.org/10.1016/j.lithos.2021.106147.

References

Barrett, T.J., MacLean, W.H., 1999. Volcanic sequences, lithogeochemistry, and hydrothermal alteration in some bimodal volcanic-associated massive sulfide systems. Rev. Econ. Geol. 8, 101–131.

Borsuk, A., Tsvetkov, A., 1982. Magmatic associations of the western part of the Aleutian Island arc. Int. Geol. Rev. 24, 317–329.

Cai, Y., Rioux, M., Kelemen, P.B., Goldstein, S.L., Bolge, L., Kylander-Clark, A.R., 2015. Distinctly different parental magmas for calc-alkaline plutons and tholeitic lavas in the central and eastern Aleutian arc. Earth Planet. Sci. Lett. 431, 119–126.

- Carr, W., Quinlivan, W., Gard Jr., L., 1970. Age and stratigraphic relations of Amchitka, Banjo Point, and Chitka Point Formations, Amchitka Island, Aleutian Islands, Alaska. Surv. Bull. 1324. A16–A22.
- Chin, E.J., Shimizu, K., Bybee, G.M., Erdman, M.E., 2018. On the development of the calcalkaline and tholeiitic magma series: a deep crustal cumulate perspective. Earth Planet. Sci. Lett. 482, 277–287.
- Citron, G., Kay, R., Kay, S.M., Snee, L., Sutter, J., 1980. Tectonic significance of early Oligocene plutonism on Adak Island, Central Aleutian Islands, Alaska. Geology 8, 375–379.
- Coats, R., 1962. Magma type and crustal structure in the Aleutian arc. Am. Geophys. Union Geophys. Monogr. 6, 92–109.
- Coombs, M.L., McGimsey, R.G., Browne, B.L., 2012. Digital database for Geologic Map of Mount Gareloi, Gareloi Island, Alaska. U.S. Geological Survey Scientific Investigation Map 3145 pamphlet 18 p., 1 sheet, scale 1:24,000. Available at. http://pubs.usgs. gov/sim/3145/.
- DeLong, S.E., McDowell, F.W., 1975. K-Ar ages from the Near Islands, western Aleutian Islands, Alaska: Indication of a mid-Oligocene thermal event. Geology 3, 691–694.
- Delong, S.E., Fox, P.J., McDowell, F.W., 1978. Subduction of the Kula ridge at the Aleutian trench. Geol. Soc. Am. Bull. 89, 83–95.
- Ducea, M.N., Barton, M.D., 2007. Igniting flare-up events in Cordilleran arcs. Geology 35, 1047–1050
- Farner, M.J., Lee, C.-T.A., 2017. Effects of crustal thickness on magmatic differentiation in subduction zone volcanism: a global study. Earth Planet. Sci. Lett. 470, 96–107.
- Ferrari, L., Valencia-Moreno, M., Bryan, S., Alaniz-Álvarez, S., Nieto-Samaniego, Á., 2007. Magmatism and tectonics of the Sierra Madre Occidental and its relation with the evolution of the western margin of North America. Spec. Pap. Geol. Soc. Am. 422, 1.
- Geist, E.L., Childs, J.R., Scholl, D.W., 1988. The origin of summit basins of the Aleutian Ridge: Implications for block rotation of an arc massif. Tectonics 7, 327–341.
- Govindaraju, K., 1994. Compilation of working values and sample description for 383 geostandards. Geostand. Geoanal. Res. 18, 1–158.
- Guilmette, C., Smit, M.A., van Hinsbergen, D.J., Gürer, D., Corfu, F., Charette, B., Maffione, M., Rabeau, O., Savard, D., 2018. Forced subduction initiation recorded in the sole and crust of the Semail Ophiolite of Oman. Nat. Geosci. 11, 688–695.
- Hart, S., Erlank, A., Kable, E., 1974. Sea floor basalt alteration: some chemical and Sr isotopic effects. Contrib. Mineral. Petrol. 44, 219–230.
- Hassan, R., Müller, R.D., Gurnis, M., Williams, S.E., Flament, N., 2016. A rapid burst in hotspot motion through the interaction of tectonics and deep mantle flow. Nature 533, 239–242.
- Hastie, A.R., Kerr, A.C., Pearce, J.A., Mitchell, S., 2007. Classification of altered volcanic island arc rocks using immobile trace elements: development of the Th–Co discrimination diagram. J. Petrol. 48, 2341–2357.
- Hein, J.R., McLean, H., 1979. Paleogene sedimentary and volcanogenic rocks from Adak Island, central Aleutian Islands, Alaska. U.S. Geological Survey Professional Paper 1126 A-J E-1-E16, pp. 1–16.
- Holbrook, W.S., Lizarralde, D., McGeary, S., Bangs, N., Diebold, J., 1999. Structure and composition of the Aleutian island arc and implications for continental crustal growth. Geology 27, 31–34.
- Ishizuka, O., Tani, K., Reagan, M.K., Kanayama, K., Umino, S., Harigane, Y., Sakamoto, I., Miyajima, Y., Yuasa, M., Dunkley, D.J., 2011. The timescales of subduction initiation and subsequent evolution of an oceanic island arc. Earth Planet. Sci. Lett. 306, 229–240.
- Janiszewski, H.A., Abers, G.A., Shillington, D.J., Calkins, J.A., 2013. Crustal structure along the Aleutian island arc: new insights from receiver functions constrained by activesource data. Geochem. Geophys. Geosyst. 14, 2977–2992.
- Jicha, B.R., Brown, F.H., 2014. An age for the Korath Range, Ethiopia and the viability of ⁴⁰Ar/³⁹Ar dating of kaersutite in Late Pleistocene volcanics. Quat. Geochronol. 21, 53–57.
- Jicha, B.R., Kay, S.M., 2018. Quantifying arc migration and the role of forearc subduction erosion in the central Aleutians. J. Volcanol. Geotherm. Res. 360, 84–99.
- Jicha, B.R., Scholl, D.W., Singer, B.S., Yogodzinski, G.M., Kay, S.M., 2006. Revised age of Aleutian Island Arc formation implies high rate of magma production. Geology 34, 661–664.
- Jicha, B.R., Scholl, D.W., Rea, D.K., 2009. Circum-Pacific arc flare-ups and global cooling near the Eocene-Oligocene boundary. Geology 37, 303–306.
- Jicha, B.R., Singer, B.S., Sobol, P., 2016. Re-evaluation of the ages of 40Ar/39Ar sanidine standards and supereruptions in the western US using a Noblesse multi-collector mass spectrometer. Chem. Geol. 431, 54–66.
- Jicha, B.R., Garcia, M.O., Wessel, P., 2018. Mid-Cenozoic Pacific plate motion change: Implications for the northwest Hawaiian Ridge and circum-Pacific. Geology 46, 939–942.
- Kay, R., 1978. Aleutian magnesian andesites: melts from subducted Pacific Ocean crust. J. Volcanol. Geotherm. Res. 4, 117–132.
- Kay, S.M., Kay, R.W., 1994. Aleutian magmas in space and time. Geol. North Am. 1, 687–722.
- Kay, S.M., Kay, R., Citron, G., 1982. Tectonic controls on tholeiitic and calc-alkaline magmatism in the Aleutian Arc. J. Geophys. Res. Solid Earth 87, 4051–4072.
- Kay, S.M., Kay, R., Citron, G., Perfit, M., 1990. Calc-alkaline plutonism in the intra-oceanic Aleutian arc, Alaska. Plutonism from Antarctica to Alaska. Geol. Soc. Am. Spec. Pap. 241, 233–255.
- Kay, S.M., Jicha, B.R., Citron, G.L., Kay, R.W., Tibbetts, A.K., Rivera, T.A., 2019. The calcalkaline Hidden Bay and Kagalaska plutons and the construction of the central Aleutian oceanic arc crust. J. Petrol. 60, 393–439.

Kelemen, P.B., Yogodzinski, G.M., Scholl, D.W., 2003. Along-strike variation in the Aleutian island arc: genesis of high Mg# andesite and implications for continental crust. Inside the subduction factory. Geophys. Monogr. Ser. 138, 223–276.

- Kuiper, K., Deino, A., Hilgen, F., Krijgsman, W., Renne, P., Wijbrans, J., 2008. Synchronizing rock clocks of Earth history. Science 320, 500–504.
- Lechler, P., Desilets, M., 1987. A review of the use of loss on ignition as a measurement of total volatiles in whole-rock analysis. Chem. Geol. 63, 341–344.
- Lee, J.-Y., Marti, K., Severinghaus, J.P., Kawamura, K., Yoo, H.-S., Lee, J.B., Kim, J.S., 2006. A redetermination of the isotopic abundances of atmospheric Ar. Geochim. Cosmochim. Acta 70, 4507–4512.
- Leeman, W.P., 1983. The influence of crustal structure on compositions of subduction-related magmas. J. Volcanol. Geotherm. Res. 18, 561–588.
- Lizarralde, D., Holbrook, W.S., McGeary, S., Bangs, N.L., Diebold, J.B., 2002. Crustal construction of a volcanic arc, wide-angle seismic results from the western Alaska Peninsula. I. Geophys. Res. Solid Earth 107 EPM 4-1-EPM 4-21.
- Ludwig, K., 2008. Manual for Isoplot 3.7. 4. Berkeley Geochronology Center Special Publication. California.
- Marlow, M.S., Scholl, D.W., Buffington, E.C., Rho Alpha, T., 1973. Tectonic history of the central Aleutian arc. Geol. Soc. Am. Bull. 84, 1555–1574.
- Marvin, R.F., Cole, J.C., 1978. Radiometric Age: Compilation A. U.S. Geological Surv., Isochron/West. 22 pp. 3–14.
- Matthews, K.J., Seton, M., Müller, R.D., 2012. A global-scale plate reorganization event at 105–100 Ma. Earth Planet. Sci. Lett. 355, 283–298.
- McLean, H., Hein, J.R., Vallier, T.L., 1983. Reconnaissance geology of Amlia Island, Aleutian Islands, Alaska. Geol. Soc. Am. Bull. 94, 1020–1027.
- Meffre, S., Falloon, T.J., Crawford, T.J., Hoernle, K., Hauff, F., Duncan, R.A., Bloomer, S.H., Wright, D.J., 2012. Basalts erupted along the Tongan fore arc during subduction initiation: evidence from geochronology of dredged rocks from the Tonga fore arc and trench. Geochem. Geophys. Geosyst. 13, Q12003. https://doi.org/10.1029/2012GC004335
- Min, K., Mundil, R., Renne, P.R., Ludwig, K.R., 2000. A test for systematic errors in ⁴⁰Ar/³⁹Ar geochronology through comparison with U/Pb analysis of a 1.1-Ga rhyolite. Geochim. Cosmochim. Acta 64, 73–98.
- Miyashiro, A., 1974. Volcanic rock series in island arcs and active continental margins. Am. J. Sci. 274, 321–355.
- Morgan, W.J., 1971. Convection plumes in the lower mantle. Nature 230, 42.
- O'connor, J.M., Hoernle, K., Müller, R.D., Morgan, J.P., Butterworth, N.P., Hauff, F., Sandwell, D.T., Jokat, W., Wijbrans, J.R., Stoffers, P., 2015. Deformation-related volcanism in the Pacific Ocean linked to the Hawaiian–Emperor bend. Nat. Geosci. 8, 393.
- Paterson, S.R., Ducea, M.N., 2015. Arc magmatic tempos: gathering the evidence. Elements 11. 91–98.
- Patriat, M., Falloon, T., Danyushevsky, L., Collot, J., Jean, M.M., Hoernle, K., Hauff, F., Maas, R., Woodhead, J.D., Feig, S.T., 2019. Subduction initiation terranes exposed at the front of a 2 Ma volcanically-active subduction zone. Earth Planet. Sci. Lett. 508, 30–40.
- Pearce, J.A., 1996. A user's guide to basalt discrimination diagrams. Trace element geochemistry of volcanic rocks: applications for massive sulphide exploration. Geol. Assoc. Can. Short Course Not. 12, 79–113.
- Pfänder, J.A., Sperner, B., Ratschbacher, L., Fischer, A., Meyer, M., Leistner, M., Schaeben, H., 2014. High-resolution 40Ar/39Ar dating using a mechanical sample transfer system combined with a high-temperature cell for step heating experiments and a multicollector ARGUS noble gas mass spectrometer. Geochem. Geophys. Geosyst. 15. 2713–2726.
- Plank, T., Langmuir, C.H., 1988. An evaluation of the global variations in the major element chemistry of arc basalts. Earth Planet. Sci. Lett. 90, 349–370.
- Reagan, M.K., Ishizuka, O., Stern, R.J., Kelley, K.A., Ohara, Y., Blichert-Toft, J., Bloomer, S.H., Cash, J., Fryer, P., Hanan, B.B., 2010. Fore-arc basalts and subduction initiation in the Izu-Bonin-Mariana system. Geochem. Geophys. Geosyst. 11, Q03X12.
- Reagan, M.K., Heaton, D.E., Schmitz, M.D., Pearce, J.A., Shervais, J.W., Koppers, A.A., 2019. Forearc ages reveal extensive short-lived and rapid seafloor spreading following subduction initiation. Earth Planet. Sci. Lett. 506, 520–529.
- Ross, P.-S., Bédard, J.H., 2009. Magmatic affinity of modern and ancient subalkaline volcanic rocks determined from trace-element discriminant diagrams. Can. J. Earth Sci. 46, 823–839.
- Sato, K., Kawabata, H., Scholl, D.W., Hyodo, H., Takahashi, K., Suzuki, K., Kumagai, H., 2016.

 ⁴⁰Ar-³⁹Ar dating and tectonic implications of volcanic rocks recovered at IODP Hole
 U1342A and D on Bowers Ridge, Bering Sea. Deep-Sea Res. II Top. Stud. Oceanogr.
 125, 214–226.
- Schaen, A.J., Jicha, B.R., Kay, S.M., Singer, B.S., Tibbetts, A., 2016. Eocene to Pleistocene magmatic evolution of the Delarof Islands, Aleutian Arc. Geochem. Geophys. Geosyst. 17, 1086–1108.
- Scholl, D.W., 2007. Viewing the tectonic evolution of the Kamchatka-Aleutian (KAT) connection with an Alaska crustal extrusion perspective. Volcanism and Subduction: The Kamchatka Region. Geophysical Monograph Series. 172, pp. 3–35.
- Scholl, D.W., Marlow, M.S., Macleod, N.S., Buffington, E.C., 1976. Episodic Aleutian Ridge igneous activity: implications of Miocene and younger submarine volcanism west of Buldir Island. Geol. Soc. Am. Bull. 87, 547–554.
- Scholl, D., Vallier, T., Stevenson, A., 1982. Arc, forearc, and trench sedimentation and tectonics; amlia corridor of the aleutian ridge: convergent margins: field investigations of margin structure and stratigraphy. In: Watkins, J.S., Drake, C.L. (Eds.), Studies in Continental Margin Geology, AAPG memoir. 34, pp. 413–439.
- Scholl, D.W., Vallier, T.L., Stevenson, A.J., 1987. Geologic evolution and petroleum geology of the Aleutian Ridge. In: Scholl, D.W., Grantz, A., Vedder, J.G. (Eds.), Geology and Resource Potential of the Continental Margin of Western North America and Adjacent Ocean Basins—Beaufort Sea to Baja California. Earth Science Series 6. Circum-Pacific Council for Energy and Mineral Resources, Houston, Texas, pp. 124–155.

- Seton, M., Müller, R., Zahirovic, S., Gaina, C., Torsvik, T., Shephard, G., Talsma, A., Gurnis, M., Turner, M., Maus, S., 2012. Global continental and ocean basin reconstructions since 200 Ma. Earth Sci. Rev. 113, 212–270.
- Sharp, W.D., Clague, D.A., 2006. 50-Ma initiation of Hawaiian-Emperor bend records major change in Pacific plate motion. Science 313, 1281–1284.
- Shillington, D.J., Van Avendonk, H.J., Holbrook, W.S., Kelemen, P.B., Hornbach, M.J., 2004. Composition and structure of the central Aleutian island arc from arc-parallel wide-angle seismic data. Geochem. Geophys. Geosyst. 5. https://doi.org/10.1029/2004GC000715.
- Singer, B.S., Myers, J.D., 1990. Intra-arc extension and magmatic evolution in the central Aleutian arc, Alaska. Geology 18, 1050–1053.
- Steinberger, B., Sutherland, R., O'connell, R., 2004. Prediction of Emperor-Hawaii seamount locations from a revised model of global plate motion and mantle flow. Nature 430, 167
- Stotz, I.L., Iaffaldano, G., Davies, D., 2017. Late Miocene Pacific plate kinematic change explained with coupled global models of mantle and lithosphere dynamics. Geophys. Res. Lett. 44, 7177–7186.
- Straub, S.M., 2003. The evolution of the Izu Bonin-Mariana volcanic arcs (NW Pacific) in terms of major element chemistry. Geochem. Geophys. Geosyst. 4, 1018.
- Tang, M., Erdman, M., Eldridge, G., Lee, C.-T.A., 2018. The redox 'filter' beneath magmatic orogens and the formation of continental crust. Sci. Adv. 4, eaar4444.
- Tarduno, J.A., Duncan, R.A., Scholl, D.W., Cottrell, R.D., Steinberger, B., Thordarson, T., Kerr, B.C., Neal, C.R., Frey, F.A., Torii, M., 2003. The Emperor Seamounts: southward motion of the Hawaiian hotspot plume in Earth's mantle. Science 301, 1064–1069.
- of the Hawaiian hotspot plume in Earth's mantle. Science 301, 1064–1069.

 Taylor, R.N., Nesbitt, R.W., Vidal, P., Harmon, R.S., Auvray, B., Croudace, I.W., 1994. Mineralogy, chemistry, and genesis of the boninite series volcanics, Chichijima, Bonin Islands, Japan. J. Petrol. 35, 577–617.
- Torsvik, T.H., Doubrovine, P.V., Steinberger, B., Gaina, C., Spakman, W., Domeier, M., 2017.

 Pacific plate motion change caused the Hawaiian-Emperor Bend. Nat. Commun. 8, 1–12.

- Tsvetkov, A.A., 1991. Magmatism of the westernmost (Komandorsky) segment of the Aleutian Island Arc. Tectonophysics 199, 289–317.
- Vaes, B., Van Hinsbergen, D.J., Boschman, L.M., 2019. Reconstruction of subduction and back-arc spreading in the NW Pacific and Aleutian Basin: clues to causes of Cretaceous and Eocene plate reorganizations. Tectonics 38, 1367–1413.
- Wanke, M., Portnyagin, M., Hoernle, K., Werner, R., Hauff, F., van den Bogaard, P., Garbe-Schönberg, D., 2012. The Bowers ridge (Bering Sea): an Oligocene–early Miocene Island Arc. Geology 40, 687–690.
- Werner, R., Hoernle, K., Hauff, K., Portnyagin, M., 2016. Origin and evolution of the Bearing Sea: an integrated geochronological, volcanological, petrological and geochemical approach, Leg1: Dutch Harbor (U.S.A.)-Petropavlovsk-Kamchatsy (Russia), 05.06.2016–15.07.2016, Leg 2: Petropavlovsk-Kamchatsky (Russia)-Tomakomai (Japan), 16.07.2016–14.08.2016. GEOMAR Report, N. Se. 030. GEOMAR Helmholtz-Zentrum für Ozeanforschung, Kiel, Germany https://doi.org/10.3289/GEOMAR_REP_NS_30_2016 451 pp.
 Wright, N.M., Seton, M., Williams, S.E., Mueller, R.D., 2016. The Late Cretaceous to recent
- Wright, N.M., Seton, M., Williams, S.E., Mueller, R.D., 2016. The Late Cretaceous to recent tectonic history of the Pacific Ocean basin. Earth Sci. Rev. 154, 138–173.
- Yogodzinski, G., Rubenstone, J., Kay, S., Kay, R., 1993. Magmatic and tectonic development of the western Aleutians: an oceanic arc in a strike-slip setting. J. Geophys. Res. Solid Earth 98, 11807–11834.
- Yogodzinski, G.M., Brown, S.T., Kelemen, P.B., Vervoort, J.D., Portnyagin, M., Sims, K.W.W., Hoernle, K., Jicha, B.R., Werner, R., 2015. The Role of Subducted Basalt in the Source of Island Arc Magmas: evidence from Seafloor Lavas of the Western Aleutians. J. Petrol. 56. 441–492.
- Yogodzinski, G.M., Kelemen, P.B., Hoernle, K., Brown, S.T., Bindeman, I., Vervoort, J.D., Sims, K.W.W., Portnyagin, M., Werner, R., 2017. Sr and O isotopes in western Aleutian seafloor lavas: Implications for the source of fluids and trace element character of arc volcanic rocks. Earth Planet. Sci. Lett. 475, 169–180.